Spatial and temporal coordination of Duox/TrpA1/Dh31 and IMD pathways is required for the efficient elimination of pathogenic bacteria in the intestine of Drosophila larvae

Fatima Tleiss, Martina Montanari, Olivier Pierre, Julien Royet, Dani Osman, Armel Gallet, C. Léopold Kurz

TITLE

Spatial and temporal coordination of Duox/TrpA1/Dh31 and IMD pathways is required for the efficient elimination of pathogenic bacteria in the intestine of *Drosophila* larvae.

AUTHORS

Fatima Tleiss[1], Martina Montanari[2], Olivier Pierre[1], Julien Royet[2]*, Dani Osman[3]*, Armel Gallet[1]* and C. Léopold Kurz[2]*

AFFILIATIONS

1 : Université Côte d'Azur, CNRS, INRAE, ISA, France

2: Aix-Marseille Université, CNRS, IBDM, Marseille, France

3: UMR PIMIT (Processus Infectieux en Milieu Insulaire Tropical) CNRS 9192- INSERM 1187-IRD 249-Université de La Réunion, île de La Réunion, France.

* Corresponding authors: e-mail: armel.gallet@unice.fr; leopold.kurz@univ-amu.fr; dani.osman@univ-reunion.fr; julien.royet@univ-amu.fr

ABSTRACT

Multiple gut antimicrobial mechanisms are coordinated in space and time to efficiently fight foodborne pathogens. In *Drosophila melanogaster*, production of reactive oxygen species (ROS) and antimicrobial peptides (AMPs) together with intestinal cell renewal play a key role in eliminating gut microbes. An alternative protective mechanism would be to selectively prevent the penetration of the intestinal tract by pathogenic bacteria while allowing colonization by commensals. Using real-time imaging to follow the fate of ingested bacteria, we demonstrate that while commensal *Lactiplantibacillus plantarum* freely enter and cross the larval midgut, pathogenic strains such as. *Erwinia carotovora* or *Bacillus thuringiensis*, are actively locked down in the anterior midgut where they are rapidly eliminated by antimicrobial peptides. This sequestration of pathogenic bacteria in the anterior midgut requires the Duox enzyme in enterocytes, and both TrpA1 and Dh31 in enteroendocrine cells. Supplementing larval food with hCGRP, the human homolog of Dh31, is sufficient to trigger lockdown, suggesting the existence of a conserved mechanism. While the IMD pathway is essential for eliminating the trapped bacteria, it is dispensable for the lockdown. Genetic manipulations impairing bacterial lockdown results in abnormal colonization of posterior midgut regions by pathogenic bacteria. This ectopic colonization leads to bacterial proliferation and larval death, demonstrating the critical role of bacteria anterior sequestration in larval defense. Our study reveals a temporal orchestration during which pathogenic bacteria, but not innocuous, are compartimentalized in the anterior part of the midgut in which they are eliminated in an IMD pathway dependent manner.

AUTHOR SUMMARY

Typically, when considering the immune response of animals to infection, we focus on classical immunity, encompassing both innate and adaptive aspects such as antimicrobials and circulating immune cells. However, a broader perspective on immunity includes additional strategies that enhance host protection, such as behavioral avoidance and internal mechanisms that restrict pathogen propagation. In our study using *Drosophila* larvae as a model, we uncovered spatially and temporally interconnected events that are crucial for effectively combating intestinal infections. Our findings reveal a two-step defense mechanism: first, the larvae rapidly discriminate between bacterial strains, effectively confining hazardous ones in the anterior section of the intestine in a process we term 'lockdown'. These locked down bacteria trigger the synthesis and release of antimicrobial peptides by the host, which ultimately eradicate the entrapped pathogens. Our experiments show that larvae capable of both initiating a lockdown and producing antimicrobial peptides withstand infections. In contrast, the absence of either one of these sequential defenses results in high mortality among the larvae, emphasizing the importance of each step and the necessity of their precise coordination in the immune response.

INTRODUCTION

One of the key avenues by which bacterial pathogens infiltrate a host is through the ingestion of contaminated food. If occurring, series of constitutive or inducible defense mechanisms come into play to limit the infection and ideally eradicate the pathogens. These defenses operate in a temporal manner, with mechanical and constitutive chemical barriers serving as the first line of defense, followed by inducible mechanisms involving the production of reactive oxygen species (ROS), the transcription, translation, and secretion of antimicrobial peptides (AMPs) as well as inter-organ signaling to cope with possible upcoming stages of infection. This temporality is evident between innate and adaptive immunity, with the former considered the primary defense line that contains and combats the threat while preparing the more subtle adaptive response.

To focus on deciphering innate immune processes, the insect *Drosophila melanogaster* has been widely and successfully used (Neyen et al., 2014; Younes et al., 2020). This model has made it possible to establish the chronology of the events involved in the defense against pathogenic bacteria. In *Drosophila,* as in all metazoans, a layer made of mucus, completed with a peritrophic membrane in insect midguts, protects the intestine lining from direct contact with pathogens (Hegedus et al., 2009; Lemaitre and Miguel-Aliaga, 2013; Pelaseyed et al., 2014). In adult *Drosophila*, a conserved immune response involving the production of ROS by Duox (Dual oxidase) enzyme in enterocytes is triggered in the intestine as early as 30 minutes after ingesting pathogenic bacteria. ROS directly damage bacterial membranes (Benguettat et al., 2018; Ha et al., 2009; Ha et al., 2005; Lee et al., 2013) but also exert an indirect effect in adults by triggering visceral spasms through the host detection of ROS mediated by the TrpA1 nociceptor and subsequent secretion of Diuretic Hormone 31 (Dh31) by enteroendocrine cells (Benguettat et al., 2018; Du et al., 2016a). Dh31 then binds its

receptor on visceral muscles, triggering contractions that expedite bacterial elimination (Benguettat et al., 2018). This pathway seems to be conserved during evolution as TrpA1 is a *Drosophila* homolog of TRP receptors that respond to noxious conditions (Ogawa et al., 2016) and Dh31 is the *Drosophila* homolog of the mammalian CGRP (Guo et al., 2021; Nässel and Zandawala, 2019). In parallel, the IMD innate immune pathway is activated following bacterial peptidoglycan detection, leading to the transcription AMP encoding genes and to the subsequent secretion of the peptides that kill bacteria (Capo et al., 2016).

In this work, using *Drosophila* larvae, we developed a real-time experimental system to trace the fate of pathogenic bacteria ingested with food. We characterized a new mechanism implicated in the lockdown and elimination of pathogenic bacteria in the anterior part of the midgut. We demonstrated that this lockdown is regulated by the ROS/TrpA1/Dh31 axis. Our results delineate a model in which bacterial trapping arises from ROS production in the intestinal lumen in response to pathogenic bacteria. These ROS compounds interact with TrpA1 in Dh31-expressing enteroendocrine cells located between the anterior and middle midgut, leading to Dh31 secretion and subsequent bacterial lockdown, suggesting the closure of a pylorus-like structure. Interestingly, we found that human CGRP can replace Dh31 in inducing the trapping of bacteria or fluorescent particles. Our findings also highlight the central role of this blockage, which acts first allowing sufficient time for the subsequent eradication of trapped pathogens by the IMD pathway and its downstream effectors. Collectively, our data unravel a finely tuned coordination between the ROS/TrpA1/Dh31 axis and the IMD pathway, enabling an effective bactericidal action of AMPs.

RESULTS

Bacterial lockdown in the anterior part of larval intestine

The translucency of *Drosophila* larvae allows for live studies of immune defense components and their coordination in eradicating pathogenic bacteria. Previously, we reported a decrease in food intake in larvae exposed to contaminated food with the Gram-negative opportunistic bacterium *Erwinia carotovora carotovora* (*Ecc15*), a process involving TrpA1 (Keita et al., 2017). Using blue food dye, we tracked food intake and observed that larvae remained blue without bacterial contaminants, while in the presence of *Ecc15*, they appeared clearer, indicating reduced food intake (Keita et al., 2017). Such a strategy was already used to identify a food-uptake cessation for larvae orally infected by *Pseudomonas entomophila* (Liehl et al., 2006). However, the assay with *Ecc15* was limited to 1h post-ingestion and using a food dye, not directly monitoring the fate of the ingested bacteria over the time. We therefore designed a protocol allowing to film the fate of fluorescent bacteria once ingested by the larvae. We tested three different fluorescent bacteria: *Ecc15-GFP* (*Ecc*), *Bacillus thuringiensis-GFP* (*Bt*, an opportunistic Gram-positive bacterium) and *Lactiplantibacillus plantarum-GFP* (*Lp*, a commensal Gram-positive bacterium). After 1 hour of feeding on contaminated media, *Ecc* and *Bt* were concentrated in the anterior midgut (Movies 1 and 2). The location of the bacteria specifically in the anterior part of the intestine following 1h exposure was confirmed when individuals from populations were imaged and counted (Fig 1A). Remarkably, tracking the GFP signal over time revealed that it remained in the anterior part of the larva and began to fade 6 hours after ingestion (Movies1 and 2; SUPP1A and SUPP1B). This fading suggests the elimination of the bacteria, while the larva continued to exhibit active movements. This pattern was observed for both *Ecc* and *Bt*. However, unlike the opportunistic bacteria *Ecc* and

Bt, *Lp* was present in the posterior compartment of the larval midgut after 1 hour of feeding and remained there throughout the 16-hour duration of our observation (Movie 3, Fig 1A and SUPP1C) (Storelli et al., 2018). To better characterize the lockdown phenomenon, we counted the ratio of larvae with trapped GFP-bacteria 1h post feeding. We found that more than 80% of the larvae had *Ecc* and *Bt* bacteria localized in the anterior part of the midgut (Fig 1A and 1B). The portion of the intestine containing the fluorescent bacteria is delimited posteriorly by an extensive turn. To confirm our findings, we dissected the intestines of larvae that had ingested the bacteria. Our analysis confirmed that *Ecc* and *Bt* were predominantly located in the anterior part of the intestines, whereas *Lp* was not, supporting our initial observations (SUPP2A). Our data collectively indicate that pathogenic bacteria, such as *Ecc* and *Bt*, are spatially confined to the anterior part of the larval midgut before their disappearance. In contrast, the commensal bacterium *Lp* is distributed throughout the midgut, persisting principally in the posterior part. This distinction underscores the different interactions and survival strategies of pathogenic versus commensal bacteria within the larval midgut.

The anterior intestinal localization of pathogenic bacteria is dose-specific and occurs rapidly

We hypothesized that the bacteria lockdown in the anterior part of the larval intestine was an active host response and might be dependent on the bacterial dose. To test this, we exposed larvae to varying concentrations of *Ecc* and *Bt* and measured the lockdown ratio. We found that a concentration of 2.10^9 *Ecc* bacteria per ml was sufficient to induce lockdown, whereas for Bt, a higher concentration of 4.10^{10} *Bt* bacteria per ml was required (Fig 2A). This dose-dependent result with *Ecc* eliciting the lockdown at a tenfold lower bacterial count than *Bt*, aligns with our previous findings that *Ecc* is more virulent than *Bt* in the *Drosophila* adult intestine (Loudhaief et al., 2017). In order to ascertain whether the bacterial concentrations

150 employed in our experiments could be representative of those encountered by larvae in the
151 absence of human manipulation, we assessed bacterial concentrations within 1 mm-sized
152 colony for both *Ecc* and *Bt* on LB agar plates. The average optical density at 600 nm (OD_{600}) for
153 these colonies was 31 for *Ecc* and 19.3 for *Bt*, corresponding to approximately 15 10^{10} *Ecc*
154 bacteria per mL and 2.8 10^{10} *Bt* bacteria per ml (data can be found in the source data file).
155 These values are consistent with the doses required in our assays to induce the lockdown
156 phenomenon (Fig 2A). For all subsequent experiments, we used 4.10^{10} bacteria per ml.

157 In previous intoxication assays, we arbitrary used a 1-hour time point to assess the
158 phenotype. However, observations of lockdown occurring within minutes suggested that this
159 response does not require *de novo* protein synthesis by the host. Shorter exposure times
160 revealed that *Ecc* was blocked in the anterior part of the intestine within 15 minutes, while *Bt*
161 showed a similar pattern beginning at 15 minutes and completing by 30 minutes (Fig 2B and
162 2C). Again, although lockdown was observed with both *Ecc* and *Bt*, *Ecc* proved to be more
163 potent in inducing this response. Based on these results, we defined 1h as our standard
164 exposure time of larvae with bacterial contaminated food.

165 Our assays typically involved groups of approximately 50 larvae to observe population-
166 level phenomena. Recent studies have suggested that larval behavior can be influenced by
167 group dynamics (Dombrovski et al., 2019; Dombrovski et al., 2017; Louis and de Polavieja,
168 2017; Mast et al., 2014). To determine whether group size affected the lockdown response,
169 we exposed groups of varying sizes to *Bt* or *Ecc* and measured the lockdown ratio. The
170 phenomenon proved robust even with a single larva exposed to contaminated food, indicating
171 that the response was not influenced by group size under our experimental conditions (Fig

2D). Based on these findings, for all subsequent experiments, we standardized the conditions using 4.10^{10} bacteria per ml, a 1-hour exposure time, and groups of at least 20 larvae.

Host TrpA1 and Dh31 are crucial for the lock down phenotype

In our previous study on larval intake of food contaminated with *Ecc* (Keita et al., 2017), we identified the gene *TrpA1* as essential in the host. The TrpA1 protein, a member of the TRP channel family, facilitates Ca2+ entry into cells at temperatures over 25°C or upon exposure to chemicals such as ROS (Du et al., 2016b; Gu et al., 2019; Guntur et al., 2015). This channel, recognized as a nociceptor (Lapointe and Altier, 2011), has been linked to intestinal muscle activity in adult *Drosophila* following *Ecc* exposure (Du et al., 2016a) and in response to ROS production by the host (Benguettat et al., 2018). We examined the role of TrpA1 during the larval response to contaminated food using $TrpA1^{[1]}$ homozygous viable mutant in an experimental setup with fluorescent *Lp*, *Ecc* or *Bt* bacteria. In this mutant larvae, while the localization of *Lp* in the posterior midgut remained unchanged, *Ecc* and *Bt* failed to be confined into the anterior midgut and were instead found in the posterior midgut. (Fig 3A, 3B, movie 4 and SUPP3A). This observation underscores that TrpA1 is necessary for the lockdown of pathogenic bacteria in the anterior midgut. Considering previous reports on visceral contraction in adult *Drosophila* involving ROS production, detection by TrpA1, and Dh31 secretion to expel bacteria (Benguettat et al., 2018; Du et al., 2016a), we wondered whether a similar ROS/TrpA1/Dh31 signaling axis is necessary in larvae to block pathogenic bacteria in the anterior midgut. Indeed, though the bacterial lockdown we observed did not expel microorganisms, it might involve muscle contractions triggered by the food contamination. Thus, we tested the lockdown ratio of $Dh31^{[KG09001]}$ homozygous viable mutants ($Dh31^{-}$) exposed to *Lp*, *Bt* or *Ecc* bacteria. In contrast to control animals, where fewer than 20% of

larvae exhibited *Ecc* or *Bt* in the posterior section of the intestine, for more than 60% of *Dh31*$^{-}$ mutant larvae, the pathogenic bacteria *Bt* or *Ecc* were localized in the posterior midgut confirming Dh31's crucial role in this mechanism (Fig 3A and 3B, movie 5 and SUPP3B). The localization of *Lp* was not affected (Fig 3B). The human Calcitonin Gene-Related Peptide (hCGRP) is the functional homolog of Dh31. Indeed, hCGRP has been shown to promote visceral muscle contractions in adult flies (Benguettat et al., 2018). To investigate whether the lockdown could be triggered without pathogenic bacteria in response to a hormone, we exposed larvae to either *Lp* or Dextran-FITC in the presence of hCGRP. While *Lp* and Dextran-FITC were normally distributed throughout the midgut, adding hCGRP to the food induced a significant lockdown (Fig 3B and 3C and movie 6). Interestingly, *Lp* locked down in the anterior midgut due to hCGRP began to be released after 6 hours (movie 6 and SUPP3), suggesting a dynamic and reversible phenomenon, likely linked to Dh31/hCGRP hormone metabolization. This demonstrates that the process could be triggered independently of the bacteria by a hormone, highlighting it as an active host mechanism.

Duox in Enterocytes and Dh31 in Enteroendocrine cells control pathogenic bacteria

The activation of TrpA1, potentially leading to the release of Dh31, (Belinskaia et al., 2023; Kondo et al., 2010; Kunst et al., 2014) could be a consequence of ROS production in the host larval midgut in response to *Ecc* or *Bt*. The larval intestine comprises two main cell populations: enterocytes (ECs) and enteroendocrine cells (EECs). In adult *Drosophila*, Dh31 is stored in EECs and is secreted in response to TrpA1 activation, a process well documented in literature (Benguettat et al., 2018; Chen et al., 2016; Veenstra et al., 2008). The role of ROS in the immunity of adult *Drosophila* intestine following infection has also been reported (Chakrabarti et al., 2012; Ha et al., 2005; Lee et al., 2013; Ryu et al., 2006). To investigate the involvement

of ROS in the larval bacterial lockdown, we focused on Duox, the primary enzyme responsible for luminal ROS production. We spatially silenced *Duox* expression using RNA interference (*UAS-Duox_IR*) driven by an ubiquitous driver (Da-Gal4), a driver specific of ECs (Mex-Gal4) or an EECs specific driver (Pros-Gal4). In parallel, using the same set of drivers, we tested the effects of cell-autonomous *Dh31* silencing using RNAi (*UAS-Dh31_IR*). Upon exposing these larvae to a food mixture contaminated with fluorescent *Ecc* or *Bt*, we assessed the lockdown ratio. Our results indicate that in larvae, Duox is essential in ECs for the lockdown of both *Ecc* and *Bt* (Fig 3D). Furthermore, silencing *Dh31* in EECs not only confirmed the mutant phenotype but also indicated that Dh31, necessary for the lockdown, is produced by EECs (Fig 3D). This data underscores the pivotal roles of Duox in ECs and Dh31 in EECs for the entrapment of pathogenic bacteria in the anterior part of the *Drosophila* larval midgut.

Absence of ROS prevents lockdown phenotype and leads to larval death

Our data demonstrating that Duox protein is necessary for the lockdown phenotype, implies that ROS generated by this enzyme are critical. The involvement of TrpA1, a known ROS sensor, further highlights the significance of these compounds in the process. To corroborate the necessity of ROS, we neutralized luminal ROS using DTT (Dithiothreitol), a potent reducing agent known for its efficacy against ROS, mixing it with the larval food (Benguettat et al., 2018). In normal conditions, larvae fed with *Bt* exhibit a lockdown of the bacteria in the anterior part of their intestine, as shown previously in FIG 1A, 1B and Fig 4A. However, when the larvae were exposed to a mixture of *Bt* and DTT, the intestinal lockdown of bacteria in the anterior midgut was abolished (Fig 4A). The effect of DTT over the lockdown phenotype was quantified using DTT mixed to Dextran-FITC in order to compare with a condition leading to an almost full posterior localization (FIG 4B). Together our results strongly suggest that the

role of Duox enzyme in producing ROS in the larval intestine is crucial, and these ROS act as key signals initiating the lockdown mechanism.

The lockdown is crucial for bacterial elimination and larval survival

Our real-time observations showed that between 6 and 8 hours after the lockdown of *Bt* or *Ecc* in the anterior midgut, the bacteria disappeared (movies 1 and movie 2, SUPP1A and SUPP1B). This led us to investigate the relationship between pathogen localization and larval survival. The hypothesis was that the disappearance of the GFP signal corresponded to the bacterial death. We therefore assessed the *Lp*, *Bt* or *Ecc* load over time in dissected midguts of control larvae previously exposed to contaminated food. Consistent with our film data, while the *Lp* load remained stable, the quantities of *Ecc* and *Bt* diminished rapidly in the intestines of control larvae, with no bacteria detectable 8 hours post-ingestion and lockdown (Fig 5A, 5B and 5C). However, in the intestines of *TrpA1*$^{[1]}$ and *Dh31*$^{-}$ mutants, the amount of *Bt* and *Ecc* increased overtime (Fig 5B and 5C). Unfortunately, we were unable to assess the bacterial load beyond 6 hours due to the deterioration of the midguts. Supporting this, in movies 4 and 5 (SUPP3A and SUPP3B), we observed that *Bt* or *Ecc* bacteria which were not locked down in the anterior part of the midgut did not disappear over time. More importantly, *TrpA1*$^{[1]}$ and *Dh31*$^{-}$ mutant larvae containing *Bt* or *Ecc* stopped to move suggesting they were dead. We confirmed the precocious death of the *TrpA1*$^{[1]}$ and *Dh31*$^{-}$ larvae fed with either *Bt* or *Ecc* compared to control animals (Fig 5D and 5E). Importantly, these mutants exhibited sustained viability overnight when fed with a mixture containing *Lp* or a bacteria-free diet (Fig 5E). Interestingly, control larvae fed a mixture of *Bt* and DTT, which neutralizes ROS and thus inhibits the lockdown, also perished (Fig 5F). This mortality was not due to DTT, as larvae fed Dextran-FITC plus DTT survived (FIG 5F). These findings suggest that, in larvae, the active

lockdown of *Bt* and *Ecc* in the anterior part of the midgut – involving a sequence of events with ROS production by Duox, TrpA1 activation by ROS, and Dh31 secretion – is essential for bacterial elimination by the host. Thus, failure to lock down pathogenic bacteria like *Ecc* or *Bt* results in their proliferation and consequent larval death.

The lockdown area is delimited by TRPA1+/Dh31+ cells and muscular structures

The above results suggest a working model involving the ROS/TrpA1/Dh31 axis in which Dh31 release from EECs leads to muscle contractions. However, unlike in adult *Drosophila*, where bacteria are expelled from the gut, in larvae, we observed a blockade mechanism. To better understand the physiology of the process, we utilized confocal microscopy to thoroughly examine larval midguts and explore the relationship between TrpA1-positive (TrpA1+) cells, anterior lockdown of the bacteria, and muscular structures. In larval midguts, TrpA1+ cells were also Dh31+, and these Dh31+ cells were identified as EECs (Pros+), typically located at the end of the anterior midgut. With the reporter line we used (*TrpA1*-Gal4/UAS-RFP), we noted an average of 3 TrpA1+/Dh31+ cells per gut (ranging from 2 to 6 cells across 14 examined guts, see source data file) (Fig 6A-6F). This observation was in agreement with our genetic and functional data linking Dh31 with EECs (FIG 3D) and suggested that TrpA1 and Dh31 operate within the same cells (Fig 6C, 6C' and 6C''). The shape of these TrpA1+ Dh31+ cells was characteristic of EECs (Fig 6A'). In agreement with a model involving an interaction of secreted ROS with TrpA1 and a subsequent local Dh31 release to act on muscles, following exposure to food contaminated with fluorescent *Bt* or *Ecc*, the bacteria were locked down in an area delimited by the anterior part of the gut and the TrpA1+ cells patch (Fig 6B). Additionally, we observed that the amount of Dh31 within Pros+ cells of larvae blocking bacteria was lower compared to those not exhibiting the lockdown, such as *TrpA1* mutant (Fig

6D and 6E). Then, we wondered whether specific muscle structures would exist close to the TrpA1+ cells in the anterior midgut. Actin labeling revealed fibrous structures on the basal side of the gut and attached to it in a transversal position (Fig 6C'' and 6F-6H'). These structures, typically lost during dissection, have been described in a report studying larval midgut peristalsis (LaJeunesse et al., 2010). Notably, the attachment points of these filaments, or tethers, corresponded with the locations of TrpA1+ cells and the boundary of the area where *Ecc* or *Bt* were confined (Fig 6C'' and 6F-H). These filaments have been described as longitudinal muscles emanating from two out of the four gastric caeca, but this might be a misinterpretation of the images generated by Lajeunesse et al. (2010). Indeed, a recent study describes these muscular structures using *in vivo* observations without dissections. Interestingly, they show that these muscles belong to a subgroup of alary muscles named TARMs (Thoracic Alary Related Muscles) (Bataillé et al., 2020). Specifically, TARMsT1 connect the anterior of the larvae to the extremities of gastric caeca, while TARMsT2 link the anterior part of the gut to the larval epidermis. Our findings support the hypothesis that the observed muscular structures close to the TrpA1+ cells are TARMsT2 (Fig 6C'', 6F-6H', SUPP 4 and movie 7). These TARMsT2 are attached to the longitudinal gut muscles and the intestine forms a loop at the attachment site (Fig 6H' and SUPP4)(Bataillé et al., 2020). The presence of Dh31+ EECs in this specific curved region of the gut close to the TARMsT2 attachment (Fig 6C'') along with our genetic and functional data lead to the hypothesis that this region may display a pyloric-like activity triggered by Dh31 (and also hCGRP) following exposure to pathogenic bacteria.

IMD pathway is mandatory for eliminating trapped bacteria

In our study, we observed that control larvae were able to kill *Ecc* and *Bt* bacteria trapped in the anterior part of the gut within 6-8 hours (movies 1 and 2 and Fig 5A-C). This finding raised

questions about the mechanism of bacterial elimination and the potential role of the IMD (Immune Deficiency) pathway in this process. While larval intestinal immunity is multifaceted, a key defense mechanism against bacteria is the production and secretion of AMPs (Hanson and Lemaitre, 2020). Previous studies have reported the production of ROS in larval guts, but this has not been directly linked to the killing of bacteria (Wu et al., 2012). In addition, we have previously shown in adult *Drosophila* that ROS on their own are not sufficient to kill bacteria (Benguettat et al., 2018). Thus, we focused our investigations on AMPs. Both *Ecc* and *Bt* possess DAP-type peptidoglycans (PGN), known to activate the IMD signaling cascade, which leads to the production of AMPs like Diptericin (Kaneko et al., 2006; Leulier et al., 2003; Stenbak et al., 2004). We used various mutants deficient in components of the IMD pathway, including PGRP-LC and PGRP-LE (PGN receptors), Dredd (an intracellular component), and Relish (a NF-κB transcription factor) (Zhai et al., 2018). Additionally, we studied a mutant, *ΔAMP14*, lacking 14 different AMPs (Carboni et al., 2022). We first assayed whether the IMD pathway was required for the lockdown phenotype upon ingestion of *Bt* or *Ecc*. While *Lp* was distributed throughout the gut of IMD pathway mutants, *Ecc* and *Bt* were confined to the anterior part of the intestine, akin to control larvae (movies 8-12, SUPP5 and SUPP6 and Fig 7A and 7B). Thus, the IMD pathway is not required for the lockdown of *Ecc* and *Bt* in larval intestines. Nevertheless, the movies suggested a death of the IMD mutant larvae despite the lockdown of either *Bt* or *Ecc*. We therefore tested the survival of these IMD pathway mutants following a 1h feeding with a mixture containing or not (water) fluorescent bacteria. While neither control animals nor the IMD pathway mutants died following a 1h feeding period with a *Lp* contaminated or non-contaminated food, all the IMD pathway mutants, including *ΔAMP14*, had a decreased survival after exposure to *Ecc* or *Bt* (Fig 7C and 7D). Thus, the IMD pathway is central for the survival of these animals with locked down bacteria in the anterior

part of the intestine. As this increased lethality in IMD pathway mutants might be related to an uncontrolled growth of the locked down *Bt* and *Ecc* bacteria, we performed CFU counting. With *Bt* and *Ecc*, while the initial inoculum was divided by 10^3 in 8h in the control larvae, the bacterial population was maintained and even increased 10-fold in IMD pathway mutants including *ΔAMP14* (Fig 7E and 7F). Additional observations from filming the fate of *Bt* and *Ecc* in IMD pathway mutant larvae confirmed these findings (movies 8-12). The GFP-bacteria, although locked down in the anterior part of the intestine, did not disappear, coinciding with larval immobility and presumed death. In conclusion, our findings illustrate that although the IMD pathway is dispensable for the initial sequestration of pathogenic bacteria, a process contingent on the ROS/TrpA1/Dh31 axis, it plays a crucial role in their subsequent elimination. Indeed, the AMPs produced following IMD pathway activation are essential for killing the trapped bacteria and ensuring larval survival (Figure 8).

DISCUSSION

Leveraging the transparency of the *Drosophila* larvae, we have successfully developed a novel real-time experimental system to monitor the fate of fluorescent bacteria ingested along with food. This methodological advancement has enabled us to unveil a previously uncharacterized physiological pathway necessary for the efficacy of the larval intestinal immune response, specifically involving enteroendocrine cells. Our research has uncovered a unique defense mechanism centered around a pylorus-like structure located in the anterior midgut, regulated by the enteroendocrine peptide Dh31. Notably, we observed that pathogenic bacteria, encompassing both Gram-positive and Gram-negative types, were confined to the anterior section of the larval intestine as early as 15 minutes post-ingestion. We determined that this intestinal lockdown of pathogenic bacteria necessitates a ROS/TrpA1/Dh31 axis initiated by Duox activity in enterocytes in response to pathogenic bacteria. We suspect the secrted ROS to interact with the TrpA1 ion channel receptor located in Dh31-expressing enteroendocrine cells adjacent to the pylorus-like structure (Figure 8). Previous studies on the interaction between ROS and TrpA1 support our hypothesis (Ogawa et al., 2016). The confining of pathogenic bacteria to the anterior part of the larval intestine is a mandatory step prior to their subsequent elimination by the IMD pathway. Intriguingly, previous studies utilizing fluorescent bacteria have already highlighted a specific localization of pathogenic bacteria in the larval gut. Bacteria such as *Ecc15*, *Pseudomonas entomophila*, *Yersinia pestis*, *Salmonella enterica serovar Typhimurium*, and *Shigella flexneri* were observed predominantly in the anterior part of the larval gut 6 hours after oral infection (Basset et al., 2000; Bosco-Drayon et al., 2012; Earl et al., 2015; Ramond et al., 2021; Vodovar et al., 2005). Our findings suggest that these bacteria can all induce ROS production by enterocytes, providing a unifying mechanism for their containment and elimination in the larval gut.

Interestingly, it has been reported that the opportunistic pathogen *Staphylococcus aureus (strain USA300)* predominantly colonizes the posterior midgut of *Drosophila* larvae, leading to the death of 93% of the larvae (Ramond et al., 2021). This strain of *S. aureus* produces high levels of detoxifying enzymes, such as catalase and superoxide dismutases, which effectively neutralize ROS. The authors suggested that the neutralization of ROS bactericidal activity by these enzymes is directly responsible for the bacterial proliferation and consequent host mortality (Ramond et al., 2021). However, considering our findings, we propose an alternative interpretation: the neutralization of ROS by these detoxifying enzymes might prevent the closure of the pylorus, thereby allowing *S. aureus* to access and establish in the posterior midgut. Our data also indicate that when pathogenic bacteria reach the posterior midgut, as observed in larvae fed with DTT or in *TrpA1* or *Dh31* mutants, larval survival is significantly jeopardized. This suggests that larval mortality could be attributed not to the inhibition of ROS in the posterior midgut but rather to the presence of bacteria in this region. In the study Ramond and colleagues (2021) involving *S. aureus*, the observation of bacterial spread into the posterior part was recorded 3 hours post-infection. It would be insightful to further investigate the dynamics of bacterial diffusion to determine whether, like other pathogens we studied, *S. aureus* is initially confined to the anterior part of the gut shortly after ingestion, specifically around 15 minutes post-infection. This could provide a broader understanding of the interplay between pathogen-specific strategies and host defense mechanisms in *Drosophila* larvae.

Our study has focused on an elbow-shaped region in the *Drosophila* larval midgut, characterized by a narrowing of the lumen and surrounded by muscular fibers. This region, where we observed a halt in transit when food is contaminated, has been aptly termed a pylorus-like due to its functional similarity to the human pyloric region. Interestingly, Bataillé et al. (2020) reported the presence of muscular fibers in this area that are part of a subgroup

of alary muscles known as TARMs (Thoracic Alary Related Muscles). Specifically, TARMsT1 connect the anterior part of the larvae to the extremities of a pair of gastric caeca, whereas TARMsT2 link the anterior part of the intestine to the larval epidermis. Our actin staining corroborates the identification of these muscles as TARMsT2, which are attached to the longitudinal muscles of the intestine, causing the intestine to form a loop at the site of attachment (Bataillé et al., 2020). The presence of Dh31-positive enteroendocrine cells (EECs) in this specific elbow-shaped region, close to the TARMsT2 attachment point, combined with our genetic and functional data, supports the hypothesis that this region exhibits pyloric-like activity. This activity is likely triggered by Dh31 or human Calcitonin Gene-Related Peptide (hCGRP) following bacterial exposure. Notably, our previous research in adult *Drosophila* showed that Dh31/hCGRP secretion induces contractions of the visceral longitudinal muscle fibers, expelling pathogenic bacteria rapidly (Benguettat et al., 2018). However, in larvae, while Dh31/hCGRP likely induces muscle contractions, the ensuing action may manifest as the closure of a pylorus, as evidenced by the observed retention of pathogenic bacteria. Importantly, in both larvae and adults, the same pathway and type of muscle fibers appear to be involved, as TARMsT2 are connected to longitudinal fibers (Figure 6H') (LaJeunesse et al., 2010). This finding is significant as it illustrates a conserved mechanism across developmental stages, albeit with different outcomes: expulsion of pathogens in adults and containment in larvae. In both cases, the overarching objective is the effective elimination of pathogens, demonstrating the versatility and adaptability of the *Drosophila* immune response.

Hence, our work shed lights on a yet to be anatomically characterized pylorus-like structure within the *Drosophila* larval gut, presenting a potential model for studying the functions and roles of mammalian pylori. Notably, CGRP (Calcitonin Gene-Related Peptide) secreting enteroendocrine cells have been identified in the mammalian pylorus, as highlighted

in research by (Kasacka, 2009) and (Bulc et al., 2018). Drawing parallels with mammalian stomachs, the pylorus is typically closed, opening only when the stomach becomes full. In exploring the functionality of the *Drosophila* pylorus-like, we considered two hypotheses: one, where it operates similarly to its mammalian counterpart, closing by default and opening in response to a full stomach, and another, where it remains open by default and closes upon detection of infected food in the intestine. Our observations with the commensal bacteria *Lp* (movie 3) suggest an initial closure of the pylorus as food accumulates in the anterior part of the intestine, followed by its opening to allow the passage of non-pathogen-contaminated food. This indicates a dynamic and responsive mechanism in the *Drosophila* gut. In contrast, when *Drosophila* larvae encounter food contaminated with pathogenic bacteria, the pylorus seems to contract, effectively blocking the passage of contaminated food into the anterior part of the intestine. This finding is significant as it not only reveals a unique physiological response in *Drosophila* larvae but also provides a basis for comparative studies with the mammalian gastrointestinal system, particularly in understanding the regulatory mechanisms governing pyloric function.

An intriguing question is why animals without a functional IMD pathway die from *Ecc* or *Bt* exposure while ROS production is still operating? Indeed, when the IMD pathway is disabled, bacteria are still confined in the anterior part of the gut, but are not effectively eliminated, resulting in larval death. This outcome strongly suggests that ROS alone are insufficient for bacterial eradication, even though they have been shown to damage and inhibit bacterial proliferation (Benguettat et al., 2018; Ha et al., 2005). However, the role of ROS in the immune response remains crucial since their timing of expression before antimicrobial peptides is likely a key factor for the efficiency of the immune response. Our findings, together with those from other studies, highlight the critical role of AMPs in fighting

444 off virulent intestinal bacteria, particularly in scenarios where ROS activity is compromised or
445 inadequate (Ramond et al., 2021; Ryu et al., 2006). Our findings emphasize the critical role of
446 the ROS/TrpA1/Dh31 axis in effectively eradicating ingested pathogens. The rapid production
447 of ROS following bacterial ingestion plays a pivotal role in closing the pylorus and retaining
448 virulent bacteria in the anterior midgut. Notably, this process does not necessitate a
449 transcriptional/translation response. In contrast, the production of antimicrobial peptides is a
450 lengthier process, involving the transcriptional activation of *AMP* genes downstream of the
451 IMD pathway, followed by their translation and secretion. The initial confinement of bacteria
452 in the anterior midgut allows time for AMPs to be produced to eliminate the trapped bacteria,
453 which is crucial for the organismal survival. This anterior lockdown is important since when
454 virulent bacteria reach the posterior midgut (in absence of ROS or in *TrpA1* or *Dh31* mutants)
455 the larvae die despite a functional IMD pathway. A key question arises: Is the posterior midgut
456 less equipped to combat bacteria? Research by (Bosco-Drayon et al., 2012) suggests that while
457 the posterior midgut can produce AMPs, this portion of the gut is predominantly dedicated to
458 the dampening the immune response, particularly through the production of amidases. This
459 permits an immune tolerance likely fostering the establishment of the commensal flora.
460 Consistent with this, we observed that commensal bacteria like *Lp* transit from the anterior to
461 the posterior midgut and persist there without compromising larval survival. Additionally, *Lp*
462 inherent resistance to AMPs (Arias-Rojas et al., 2023) further underscores the idea that the
463 anterior midgut serves as a checkpoint where certain bacteria are detained and eliminated,
464 while others, like *Lp*, are permitted to pass through. When the lockdown mechanism is
465 compromised, pathogens or pathobionts can spread into the posterior midgut, potentially
466 eliciting an inadequate dampened immune response. Thus, the anterior midgut acts as a
467 critical juncture in determining the fate of ingested bacteria, either leading to their elimination

or allowing their passage to the posterior midgut, where a more tolerant immune environment prevails.

Understanding the practical application of this defense mechanism in the natural environment of *Drosophila melanogaster* larvae is crucial. In the wild, *Drosophila* adults are typically drawn to rotting fruits on which they lay eggs, exposing them and their progeny to a plethora of fungi and bacteria. Consequently, developing larvae feed and grow in these non-sterile conditions. In such environments, encountering pathogenic microbes is inevitable. Evasion or avoidance behavior has been documented as a potential strategy for dealing with pathogens (Surendran et al., 2017). This behavior might enable larvae to seek environments that will supposedly better sustain their survival. However, given the larvae constant consumption of their surrounding media in a race to reach pupation, ingestion of pathogen-contaminated food is a common risk. Under these circumstances, larvae have limited options prior to the activation of their innate immune response. Discriminating innocuous from potentially deleterious bacteria and then locking down the latter ones for subsequent elimination by AMPs, clearly benefits the host. Nonetheless, the effectiveness of this lockdown strategy would be maximized if it were coordinated with evasion behaviors. Such coordination could prevent repeated engagement in this energy-intensive immune response, thus optimizing the larvae chances of reaching pupation successfully. This interplay between immune response and behavioral adaptation underlines the sophisticated strategies employed by *Drosophila* larvae to navigate their microbial-rich environment.

MATERIALS AND METHODS

1-Bacterial strain

We used the following strains: *Bacillus-thuringiensis*-GFP (*Bt*) (Hachfi et al., 2023) (the original strain, 4D22, is from the Bacillus Genetics Stock Center - www.bgsc.org), *Erwinia carotovora* subsp. *carotovora*-GFP *15* (*Ecc*) (Basset et al., 2000) and *Lactiplantibacillus plantarum*-GFP (*Lp*) (gift from Renata Matos and François Leulier) (Storelli et al., 2018). *Bt* and *Ecc* were grown on standard LB agar plates at 30°C and *Lp* was grown in MRS medium in anaerobic conditions at 37°C for at least 18 hours. Each bacterium was plated from glycerol stocks for each experiment. A single colony was used to prepare liquid cultures. Bacteria were inoculated in the 500 ml of appropriate medium. After overnight growth, the cultures were centrifuged for 15 min at 7500 rpm. Bacterial infectious doses were adjusted by measuring culture turbidity at an optical density of 600 nm. OD_{600}=100 for *Lp* and *Ecc* corresponds to $4.9.10^{7}$CFU/µl. OD_{600}=100 for *Bt* corresponds to $1,5.10^{7}$CFU/µl.

2-FLY Stocks

Flies were maintained at 25 °C on our standard fly medium (Nawrot-Esposito et al., 2020) with12:12 light/dark cycle. Fly stocks used in this study and their origins are as follows: as a reference in our experiments and noted as *ctrl*, we used Canton S (Bloomington #64349), $TrpA1^{1}$ (Bloomington #26504), $Dh31^{KG09001}$ (Bloomington #16474), *Dh31-Gal4* (Bloomington #51988), $PGRP\text{-}LC^{\Delta E}$ (Bloomington #55713), $PGRP\text{-}LE^{112}$ (Bloomington #33055), $Dredd^{F64}$ (Gift from B. Charroux), $Relish^{E20}$ (Bloomington #55714), *ΔAMP14* (Gift from B. Lemaitre; (Carboni et al., 2022), *TrpA1*-Gal4/UAS-RFP (Gal4 is Bloomington #527593, UAS is Bloomington #27392), *Da*-Gal4 (Bloomington #55851), *pros*-Gal4 (gift form B. Charroux), *Mex*-Gal4 (gift from B. Charroux), UAS-*Duox _IR* (Bloomington #38907), UAS-*Dh31_IR*(Bloomington#25925).

3-Infection experiments

Oral infections were performed on mid-L3 larvae (3.5 days after egg laying). For each experiment, between 20 and 50 non-wandering L3 larvae raised at 25°C were collected and washed in PBS (1x). Bacterial pellets were mixed with yeast 40% in PBS (1x) and 500 µl of the infected food were added at the bottom of an empty plastic fly vial (VWR) before adding the larvae and sealing it with Parafilm. Then, the larvae were placed at 25°C in the dark. After 60min, the larvae were washed in PBS (1x) and then counted for the presence of GFP-bacteria or for other analyses.

4-Larvae dissection

After 60 min, the infected larvae were washed in PBS (1x). Guts were dissected and fixed in formaldehyde 4% for 45 min, then washed twice in PBS (1x) for 10 min. Guts were mounted between poly-L-lysine (SIGMA P8920-100ML) coated slides and coverslips in Vectashield/DAPI (Vector Laboratories).

5- Colony-forming unit (CFU) counting

Infected animals were washed in ethanol 70% for 30s then rinsed in PBS (1x). Guts were dissected in PBS (1x) and homogenized with a micropestle in 200 µl of LB medium. Samples were serially diluted in LB medium and plated on LB agar plates overnight at 30 °C. The Colonies Forming Unit (CFU) were counted the following day. CFU counting has been performed at 5 time points: 1h, 2h, 4h, 6h and 8h after a 60 min intoxication (at least 20 larvae per point and 3 independent repeats).

6-Mortality test

Oral infection of the Larvae was performed as described above. Larvae of the different genotypes fed 1h with *Bt*, *Lp* or *Ecc* were quickly washed in 70% ethanol and then PBS (1x). Only the larvae that eaten (containing GFP bacteria in their intestine) were selected and put in water for 18h at 25°C. Mortality was evaluated at this time-point.

7- DTT and CGRP feeding

Oral infection of the Larvae was performed as described above.

DTT: DTT was added to the food at a final concentration of 100 nM and larvae were fed during 60 min.

hCGRP: hCGRP (Sigma #C0167) was resuspended in distilled water. Larvae were fed 1h as described above with a final hCGRP concentration of 400 µg/ml.

8-Immunostaining

Dissected intestines were washed twice with PBS (1x)-0.1% Triton X100 then incubated for 3h in the blocking solution (10% of fetal calf serum, 0.1% Triton X100, PBS (1x)). The blocking solution was removed and the primary antibodies added and incubated overnight à 4°C in blocking solution. The following antibodies were used: mouse anti-Prospero (MR1A-c, Developmental Studies Hybridoma Bank (DSHB)) at 1:200 and rabbit anti-Dh31 (gift from Jan Veenstra and Michael Nitabach; (Kunst et al., 2014; Park et al., 2008) at 1:500. Secondary antibodies used were anti-mouse Alexa647 (Invitrogen Cat# A-21235), anti-rabbit Alexa546 (Invitrogen Cat# A-11010). All secondary antibodies were used at 1:1000. Guts were mounted in Fluoroshield-DAPI mounting medium (Sigma F6057). Observations of GFP producing bacteria and of dTRPA1+ cells were done using the native fluorescence without immunostaining.

9-RNAi experiments

All the tested animals were F1 obtained from a cross between parents possessing the Gal4 transgene and parents possessing the UAS-RNAi construction or from crosses between control flies and transgenic animals. The larvae were then fed with contaminated food as described above.

10-Images and movie acquisition

Images acquisition was performed at the microscopy platform of the Institut Sophia Agrobiotech (INRAE 1355-UCA-CNRS 7254-Sophia Antipolis) with the macroscope Zeiss AxioZoom V16 with an Apotome 2 or a Zeiss Axioplan Z1 with Apotome 2 microscope. Images were analyzed using ZEN and Photoshop softwares. Movie acquisitions were performed with the macroscope Zeiss AxioZoom V16 equipped with the Hamamatsu Flash 4LT Camera. Larvae were captured every 5 minutes. Dead larva images were acquired with a numeric Keyence VHX 2000 microscope.

11-Data representation and statistical analyses

The Graphpad Prism 8 software was used for statistical analyses.

CFU data analysis: the D'Agostino–Pearson test to assay whether the values are distributed normally was applied. As not all the data sets were considered normal, non-parametric statistical analysis such as non-parametric unpaired Mann–Whitney two-tailed tests was used for all the data presented.

Lockdown ratio and survival ratio datasets: as the values obtained from one larva are categorical data with a *Yes* or *No* value, we used the two-sided Fisher exact t-test and the 95% confidence interval to test the statistical significance of a possible difference between a test sample and the related control.

For all the quantitative assays, at least 3 independent experiments were performed and some were done in two different laboratories by more than one experimenter. The results from all the experiments were gathered and the total amount of larvae tested is indicated in the source data file. In addition, we do not show the average response from one experiment representative of the different biological replicates, but an average from all the data generated during the independent experiments in one graph.

12-Source data files: detailed lines, conditions and statistics for the figure section

A file containing raw data, all the details about the experiments including the replicates, sample size, genotypes and detailed statistical analyzes is available (https://figshare.com/articles/dataset/Tleiss_et_al_lockdown_Source_Data_File/25018352 DOI:10.6084/m9.figshare.25018352).

590 **FIGURE LEGENDS**

591 **FIGURE 1**

592 **Contrary to *Lp*, *Ecc* or *Bt* bacteria are locked down in the anterior part of the gut.**

593 **A**: Pictures to illustrate the position of the green fluorescence of control L3 stage larvae as a
594 group (upper panel) or individual (lower panel) after having been fed 1h with a media
595 containing yeast and GFP-producing bacteria (*Ecc* or *Bt* or *Lp*). The white asterisk indicates the
596 anterior part of the animal. The white arrow indicates the posterior limit of the area containing
597 the fluorescent bacteria. Below the pictures are schematics representing larvae, their gut, and
598 the relative position of the GFP-producing bacteria in green. Scale bar is 1mm.

599 **B**: Graphic representing the lockdown ratio for L3 larvae exposed during 1h to a mixture
600 composed of yeast and fluorescent bacteria. The ratio of control larvae with a distinguishable
601 green fluorescence only in the upper part of the intestine, considered as locked-down
602 bacteria, is represented. The ratio is calculated as: x larvae with bacteria locked down/ (x
603 larvae with bacteria locked down + y larvae with bacteria all along the gut). Larvae with no
604 distinguishable fluorescence were considered as non-eaters and discarded from the
605 quantifications. The ratio of larvae with no distinguishable fluorescence was not influenced by
606 the different conditions we tested. Shown is the average lockdown ratio with a 95%
607 confidence interval from at least 3 independent assays with at least 30 animals per condition
608 and trial. **** indicates p<0,0001, Fischer exact t-test. See the source data file for details.

609

610

FIGURE 2

Bacterial lockdown is dose-dependent, occurs in less than 30 minutes, and does not involve a group effect.

A: Lockdown ratio for control L3 larvae fed 1h with a mixture combining yeast with different concentrations of fluorescent *Ecc* or *Bt*, concentrations are in number of bacteria per ml. Shown is the average lockdown ratio with a 95% confidence interval from at least 3 independent assays with at least 18 animals per condition and trial. **** indicates p<0,0001, Fischer exact t-test. See the source data file for details.

B: Representative images of control larvae fed during 30 min. with *Bt*. Scale bar is 1mm.

C: Lockdown ratio for control L3 larvae fed during various times with a mixture combining yeast with *Ecc* or *Bt.* Shown is the average lockdown ratio with a 95% confidence interval from at least 3 independent assays with at least 20 animals per condition and trial. ns indicates values with differences not statistically significant, **** indicates p<0,0001, Fischer exact t-test. See the source data file for details.

D: Lockdown ratio for control L3 larvae fed 1h as individual animals or as groups of 10 or >40 with a mixture combining yeast with a constant concentration of *Ecc* or *Bt* (4.10^{10} bacteria per ml). Shown is the average lockdown ratio with a 95% confidence interval from at least 3 independent assays with the exact number of animals indicated per condition and trial. ns indicates values with differences not statistically significant, Fischer exact t-test. See the source data file for details.

FIGURE 3

The bacterial lockdown necessitates Duox in enterocytes, the TrpA1 nociceptor and Dh31 in enteroendocrine cells.

A: Pictures to illustrate the localization of the fluorescent bacteria within the intestine of control (ctrl), *Trpa1*$^{[1]}$ or *Dh31*$^{-}$ L3 larvae after having been fed 1h with a mixture of yeast and *Ecc*. Scale bar is 1mm.

B: Lockdown ratio for control (ctrl) L3 larvae or mutants for *Trpa1*$^{[1]}$ or *Dh31*$^{-}$ fed 1h with a mixture combining yeast and *Lp* or *Ecc* or *Bt* or fluorescent Dextran with or without hCGRP hormone. Shown is the average lockdown ratio with a 95% confidence interval from at least 3 independent assays with at least 30 animals per condition and trial. 0 indicates an absence of lockdown. **** indicates p<0,0001, Fischer exact t-test. See the source data file for details.

C: Pictures to illustrate the localization of the fluorescence within the intestine of control L3 larvae after having been fed 1h with a mixture of yeast and fluorescent Dextran with or without hCGRP hormone. Below the pictures are schematics representing larvae, their gut, and the relative position of the fluorescence in green. Scale bar is 1mm.

D: Lockdown ratio for animals expressing RNA interference constructions directed against *Duox* mRNA or *Dh31* mRNA, ubiquitously (Da-Gal4), in enterocytes (Mex-Gal4) or in enteroendocrine cells (Pros-Gal4) and then fed 1h with a mixture combining yeast and *Ecc* or *Bt*. Shown is the average lockdown ratio with a 95% confidence interval from at least 3 independent assays with at least 30 animals per condition and trial. ns indicates values with differences not statistically significant, **** indicates p<0,0001 , Fischer exact t-test. See the source data file for details.

655 **FIGURE 4**

656 **Blocking the ROS with DTT prevents the lockdown of *Bt* and the larvae with bacteria in the**
657 **posterior part of the intestine die.**

658 **A**: Pictures to illustrate the localization of the fluorescence within the intestine of control
659 (ctrl) L3 larvae after having been fed 1h with a mixture of yeast and *Bt* with or without DTT.
660 Below the pictures are schematics representing larvae, their gut, and the relative position of
661 the fluorescent bacteria in green. Scale bar is 1mm.

662 **B**: Lockdown ratio for control (ctrl) L3 larvae fed 1h with a mixture combining yeast, DTT and
663 fluorescent Dextran or *Bt*. Shown is the average lockdown ratio with a 95% confidence interval
664 from at least 3 independent assays with at least 18 animals per condition and trial. ns indicates
665 values with differences not statistically significant, Fischer exact t-test. See the source data file
666 for details.

667

FIGURE 5

In the absence of lockdown in *TrpA1*$^{[1]}$ or *Dh31*$^{-}$ mutants, *Bt* and *Ecc* proliferate in the larval intestine and the larvae die.

A, **B** and **C**: quantification over time of the amount of *Lp*, (A), *Bt* (B) or *Ecc* (C) live bacteria within the larval intestine of control (ctrl) (A, B and C), *Dh31*$^{-}$ (B and C) and *TrpA1*$^{[1]}$ (B and C) animals following a 1h feeding period with a solution containing yeast and bacteria. CFU stands for Colony Forming Units. Shown is the average ± SEM of at least 3 independent experiments with at least 7 guts each. After 8h, either all the *TrpA1*$^{[1]}$ or *Dh31*$^{-}$ larvae were dead or the intestines were severely damaged preventing the CFU counting. * Indicates p<0,05, Mann Whitney, two-tailed test. See the source data file for details.

D: Pictures of control (ctrl) or *TrpA1*$^{[1]}$ or *Dh31*$^{-}$ larvae after 8h in water following a 1h feeding with a mixture of yeast and *Bt.* For control larvae, some animals made pupae that are visible while for *TrpA1*$^{[1]}$ and *Dh31*$^{-}$mutants, the dark larvae are dead non-moving melanized animals. Scale bar is 1mm.

E: Ratio of dead control or T*rpA1*$^{[1]}$ or *Dh31*$^{-}$ larvae after 8h in water following or not (water) a 1h feeding period with yeast mixed with *Lp* or *Ecc* or *Bt.* Shown is the average with 95% confidence interval of at least 3 independent experiments with at least 21 larvae per trial and condition. The 0 symbol indicates an absence of lethality. **** indicates p<0,0001, Fischer exact t-test. See the source data file for details.

F: Ratio of dead control (ctrl) larvae after 8h in water following a 1h feeding period with a mixture combining yeast, DTT and Dextran fluorescent beads or *Bt*. Shown is the average with 95% confidence interval of at least 3 independent experiments with at least 18 larvae per trial

690 and condition. The 0 symbol indicates an absence of lethality. **** indicates p<0,0001, Fischer

691 exact t-test. See the source data file for details.

692 **FIGURE 6**

693 **TrpA1+ cells are enteroendocrine cells concentrated in a portion of the intestine bordering**
694 **the locked-down bacteria.**

695 Confocal fluorescent pictures of the anterior portions of L3 larval intestines to detect;
696 longitudinal and transversal muscles concentrated in actin (F, G, H and H'), TrpA1+ cells
697 producing RFP (A, A', B, C, C'' and F), GFP-bacteria (B, G and H), Dh31+ cells (C', C'', D and E),
698 Pros+ cells (D and E) and nuclei with DNA staining (A, A', B, C'', D, E and G).

699 In B, D, E, G, H and H'; animals were previously fed for 1h with a mixture containing bacteria
700 and yeast with *Bt* (B, D and E) or *Ecc* (G, H and H'). When present, the white star indicates the
701 anterior part of the intestinal portion shown, the arrows point to TARMs and the > symbols
702 point to TrpA1+ cells. The empty squares in A and H with dashed lines correspond to the
703 portion of the image magnified in A' and H', respectively. Scale bar in A, B, F, G and H
704 represents 500µm, in A', C, D, E and H' represents 100 µm.

705

706 **FIGURE 7**

707 **IMD pathway is not required for the lockdown but essential for larvae survival and *Bt* or *Ecc***
708 **clearance**

709 **A**: Pictures to illustrate the localization of the fluorescence within the intestine of *PGRP-*
710 *LC*$^{[\Delta E]}$ L3 larvae after having been fed 1h with a mixture of *Lp* or *Ecc* or *Bt*. Scale bar is 1mm.

711 **B**: Lockdown ratio for control L3 larvae or mutants of the IMD pathway fed 1h with a mixture
712 combining yeast and *Lp* or *Ecc* or *Bt*. Shown is the average with 95% confidence interval of at
713 least 3 independent experiments with at least 20 larvae per trial and condition. ns indicates
714 values with differences not statistically significant, Fischer exact t-test. See the source data file
715 for details.

716 **C**: Pictures of *PGRP-LC*$^{[\Delta E]}$, *Rel*$^{[E20]}$ or *ΔAMP14* mutant larvae after 18h in water following a 1h
717 feeding with a mixture of yeast and *Bt*. The dark larvae are dead non-moving melanized
718 animals. *ΔAMP14* is a mutant deleted for 14 antimicrobial-encoding genes.

719 **D**: Ratio of dead control or *TrpA1*$^{[1]}$ or *Dh31*$^{-}$ larvae after 18h in water following or not (water)
720 a 1h feeding period with yeast mixed with *Lp* or *Ecc* or *Bt*. Shown is the average with 95%
721 confidence interval of at least 3 independent experiments with at least 20 larvae per trial and
722 condition. The 0 symbol indicates an absence of lethality. **** indicates p<0,0001, Fischer
723 exact t-test. See the source data file for details.

724 **E** and **F**: quantification over time of the amount of *Bt* (A) and *Ecc* (B) live bacteria within the
725 larval intestine of control or IMD pathway mutant animals including *ΔAMP14* following a 1h
726 feeding period with a solution containing yeast and bacteria. CFU stands for Colony Forming
727 Units. *ΔAMP14* is a mutant deleted for 14 antimicrobial-encoding genes. Shown is the average

± SEM of at least 3 independent experiments with at least 7 guts each. After 8h, either all the mutants were dead or the intestines were severely damaged preventing the CFU counting. * Indicates p<0,05, Mann Whitney, two-tailed test. See the source data file for details.

FIGURE 8

Chronological coordination of ROS/TrpA1/Dh31 and IMD pathways for an efficient microbial elimination

t0: larvae ingest bacteria from the food mixture (anterior on the left, only bacteria similar to *Ecc* or *Bt* are illustrated). This initial phase necessitates a discrimination between commensal and pathogenic bacteria, not elucidated in this study (symbolized by '?'). The presence of pathogenic bacteria induces the production of ROS by enterocytes (EC) in a Duox-dependent manner. Then ROS activates TrpA1 in enteroendocrine cells (EEC). **t15 minutes:** Dh31 secretion by EEC is responsible for the lockdown of bacteria likely by promoting visceral muscle contractions leading to a closure of a pylorus-like structure. This phenomenon concentrates the bacteria in the anterior part of the gut. The bacterial concentration in this part of the intestinal lumen may facilitate the triggering of the IMD signaling cascade that controls the transcription of the genes (*AMPs*) encoding the antimicrobial peptides (AMPs). **t6 hours:** the pylorus-like structure is still closed. The bactericidal activity of AMPs has eliminated most of the bacteria accumulated in the anterior part of the intestine. Importantly, if confinement is prevented, the larvae die; if the response by antimicrobial peptides is hindered, the larvae die.

752 **SUPP1**

753 ***Ecc* and *Bt* are locked down in the anterior part of the intestine and disappear while *Lp***
754 **transits to the posterior part and remains.**

755 **A**: Timelapse from the movies of L3 Larvae fed 1h with a mixture of yeast and *Ecc* then
756 transferred on a glass slide to be imaged overnight. Refers to Movie 1.

757 **B**: Timelapse from the movies of L3 Larvae fed 1h with a mixture of yeast and *Bt* then
758 transferred on a glass slide to be imaged overnight. Refers to Movie 2.

759 **C**: Timelapse from the movies of L3 Larvae fed 1h with a mixture of yeast and *Lp* then
760 transferred on a glass slide to be imaged overnight. Refers to Movie 3.

761 For A-C, the frames are separated by 5 minutes.

762 **SUPP2**

763 **Contrary to *Lp*, *Ecc* or *Bt* bacteria are locked down in the anterior part of the gut.**

764 **A**: Graphic representing the lockdown ratio for dissected intestines of L3 larvae exposed
765 during 1h to a mixture composed of yeast and fluorescent bacteria. Shown is the average
766 lockdown ratio with a 95% confidence interval from at least 3 independent assays with at least
767 8 organs per condition and trial. **** indicates p<0,0001, Fischer exact t-test. See the source
768 data file for details.

769

770 **SUPP3**

771 ***Ecc* is not locked down anteriorly in *TrpA1*$^{[1]}$ and *Dh31*$^{-}$ mutants, persists in the posterior**
772 **part of the intestine and disappear while *Lp* can be locked down following exogenous**
773 **addition of hCGRP.**

774 **A**: Timelapse from the movies of *TrpA1*$^{[1]}$ L3 Larvae fed 1h with a mixture of yeast and *Ecc*
775 then transferred on a glass slide to be imaged overnight. Refers to Movie 4.

776 **B**: Timelapse from the movies of *Dh31*$^{-}$ L3 Larvae fed 1h with a mixture of yeast and *Ecc* then
777 transferred on a glass slide to be imaged overnight. Refers to Movie 5.

778 **C**: Timelapse from the movies of w^{-} L3 Larvae fed 1h with a mixture of yeast and *Lp* + hCGRP
779 then transferred on a glass slide to be imaged overnight. Refers to Movie 6.

780 For A-C, the frames are separated by 5 minutes.

781

SUPP4

Confocal fluorescent pictures of different TARMsT2 in the anterior portions of L3 larval intestines to detect longitudinal and transversal muscles concentrated in actin The white star indicates the anterior part of the intestinal portion shown. The empty square with dashed lines in A corresponds to the portion of the image magnified in A'. Scale bar represents 500µm.

SUPP5

***Bt* and *Ecc* are locked down anteriorly and persist in *PGRP-LC*$^{[\Delta E]}$ *and PGRP-LE*$^{[112]}$ mutants, respectively.**

A: Timelapse from the movies of *PGRP-LC*$^{[\Delta E]}$ L3 Larvae fed 1h with a mixture of yeast and *Bt* then transferred on a glass slide to be imaged overnight. Refers to Movie 8.

B: Timelapse from the movies of *PGRP-LE*$^{[112]}$ L3 Larvae fed 1h with a mixture of yeast and *Ecc* then transferred on a glass slide to be imaged overnight. Refers to Movie 9.

For A and B, the frames are separated by 5 minutes.

797 **SUPP6**

798 ***Bt* and *Ecc* are locked down and persist anteriorly in *Dredd*$^{[F64]}$ *and Rel*$^{[E20]}$ mutants.**

799 **A**: Timelapse from the movies of *Dredd*$^{[F64]}$ L3 Larvae fed 1h with a mixture of yeast and *Ecc*

800 then transferred on a glass slide to be imaged overnight. Refers to Movie 10.

801 **B**: Timelapse from the movies of *Rel*$^{[E20]}$ L3 Larvae fed 1h with a mixture of yeast and *Bt* then

802 transferred on a glass slide to be imaged overnight. Refers to Movie 11.

803 **C**: Timelapse from the movies of *Rel*$^{[E20]}$ L3 Larvae fed 1h with a mixture of yeast and *Ecc* then

804 transferred on a glass slide to be imaged overnight. Refers to Movie 12.

805 For A-C, the frames are separated by 5 minutes.

806

807

MOVIES

Movie 1

https://figshare.com/articles/media/ctrl_vs_Ecc-gfp/25018385

DOI: 10.6084/m9.figshare.25018385

Fluorescent *Ecc* is locked down in the anterior part of the larval intestine then vanishes.

Live imaging during 12h of a L3 control larva previously fed 1h with a food containing *Ecc* fluorescent bacteria then transferred on a glass slide in a wet chamber.

Movie 2

https://figshare.com/articles/media/2-ctrl_vs_Bt-GFP/25018427

DOI: 10.6084/m9.figshare.25018427

Fluorescent *Bt* is locked down in the anterior part of the larval intestine then vanishes.

Live imaging during 12h of a L3 control larva previously fed 1h with a food containing *Bt* fluorescent bacteria then transferred on a glass slide in a wet chamber.

Movie 3

https://figshare.com/articles/media/Tleiss_et_al_Movie_3-ctrl_vs_Lp_avi/25018442

DOI: 10.6084/m9.figshare.25018442

Fluorescent *Lp* is not locked down in the anterior part of the larval intestine and persists in the posterior midgut.

828 Live imaging during 10h of a L3 control larva previously fed 1h with a food containing *Lp*
829 fluorescent bacteria then transferred on a glass slide in a wet chamber.

830

831 **Movie 4**

832 **https://figshare.com/articles/media/Tleiss_et_al_Movie_4_TrpA1_vs_Ecc-gfp/25018463**

833 **DOI :10.6084/m9.figshare.25018463**

834 **Fluorescent *Ecc* is not locked down in the anterior part of the *TrpA1* mutant larval intestine**
835 **and persists in the posterior midgut.**

836 Live imaging during 10h of a L3 *TrpA1* mutant larva previously fed 1h with a food containing
837 *Ecc* fluorescent bacteria then transferred on a glass slide in a wet chamber.

838

839 **Movie 5**

840 **https://figshare.com/articles/media/Tleiss_et_al_Movie_5_Dh31_vs_Ecc/25018472**

841 **DOI: 10.6084/m9.figshare.25018472**

842 **Fluorescent *Ecc* is not locked down in the anterior part of the *Dh31* mutant larval intestine**
843 **and persists in the posterior midgut.**

844 Live imaging during 10h of a L3 *Dh31* mutant larva previously fed 1h with a food containing
845 *Ecc* fluorescent bacteria then transferred on a glass slide in a wet chamber.

846

847

Movie 6

https://figshare.com/articles/media/Tleiss_et_al_Movie_6_ctrl_vs_Lp_vs_hCGRP/25018481

DOI: 10.6084/m9.figshare.25018481

Fluorescent *Lp* is locked down in the anterior part of the larval intestine following treatment with hCGRP.

Live imaging during 12h of a control L3 larva previously fed 1h with a food containing *Lp* fluorescent bacteria and hCGRP then transferred on a glass slide in a wet chamber.

Movie 7

https://figshare.com/articles/media/Tleiss_et_al_Movie_7_TARM_T2_3D/25018496

DOI: 10.6084/m9.figshare.25018496

TARMsT2 are attached to the longitudinal gut muscles.

Confocal imaging of the intestine from a control animal stained with fluorescent phalloidin and animated 3D-reconstruction of the anterior portion containing the attached TARMs.

Movie 8

https://figshare.com/articles/media/Tleiss_et_al_Movie_8_pgrp-lc_vs_Bt/25018499

DOI :10.6084/m9.figshare.25018499

867 **Fluorescent *Bt* is locked down in the anterior part of the *PGRP-LC* mutant larval intestine**
868 **and persists.**

869 Live imaging during 12h of a L3 *PGRP-LC* mutant larva previously fed 1h with a food containing
870 *Bt* fluorescent bacteria then transferred on a glass slide in a wet chamber.

871

872 **Movie 9**

873 **https://figshare.com/articles/media/Tleiss_et_al_Movie_9_pgrp-le_vs_Ecc/25018505**

874 **DOI: 10.6084/m9.figshare.25018505**

875 **Fluorescent *Ecc* is locked down in the anterior part of the *PGRP-LE* mutant larval intestine**
876 **and persists.**

877 Live imaging during 12h of a L3 *PGRP-LE* mutant larva previously fed 1h with a food containing
878 *Ecc* fluorescent bacteria then transferred on a glass slide in a wet chamber.

879

880 **Movie 10**

881 **https://figshare.com/articles/media/Tleiss_et_al_Movie_10_Dredd_vs_Ecc/25018517**

882 **DOI: 10.6084/m9.figshare.25018517**

883 **Fluorescent *Ecc* is locked down in the anterior part of the *Dredd* mutant larval intestine and**
884 **persists.**

885 Live imaging during 12h of a L3 *Dredd* mutant larva previously fed 1h with a food containing
886 *Ecc* fluorescent bacteria then transferred on a glass slide in a wet chamber.

887

888 **Movie 11**

889 https://figshare.com/articles/media/Tleiss_et_al_Movie_11_Rel_vs_Bt/25018529

890 **DOI: 10.6084/m9.figshare.25018529**

891 **Fluorescent *Bt* is locked down in the anterior part of the *Rel* mutant larval intestine and**
892 **persists.**

893 Live imaging during 12h of a L3 *Rel* mutant larva previously fed 1h with a food containing *Bt*
894 fluorescent bacteria then transferred on a glass slide in a wet chamber.

895

896 **Movie 12**

897 https://figshare.com/articles/media/tleiss_et_al_Movie_12_Rel_vs_Ecc/25018538

898 **DOI: 10.6084/m9.figshare.25018538**

899 **Fluorescent *Ecc* is locked down in the anterior part of the *Rel* mutant larval intestine and**
900 **persists.**

901 Live imaging during 12h of a L3 *Rel* mutant larva previously fed 1h with a food containing *Ecc*
902 fluorescent bacteria then transferred on a glass slide in a wet chamber.

903

904

905

AUTHOR CONTRIBUTIONS

L.K., A.G., F.T., M.M., O.P., D.O. and J.R. conceived the experiments. F.T., M.M., O.P. performed the experiments. L.K., A.G., F.T., D.O. and J.R. wrote the manuscript. A.G., D.O. and J.R. secured funding.

COMPETING INTERESTS

The authors have declared that no competing interests exist.

ACKNOWLEDGMENTS

We are grateful to all members of the BES and DEB teams at the Institut Sophia Agrobiotech for fruitful discussions. We greatly thank Emilie Avazéri, Gladys Gazelle, Marie-Paule Esposito, Juliette Dubois and Elisa Di Lelio for their technical support. We thank Bernard Charroux (at the IBDM Aix Marseille University) and Ambra MASUZZO (in the team of Richard Benton, Université de Lausanne) for pioneer observations and numerous discussions, François Leulier and Renata Matos for sharing bacterial and fly lines and Frank Schnorrer for discussions about alary muscles.

FUNDING

F.T. was supported by the Lebanese Association for Scientific Research (LASER), the AJAJE association from Lebanon, and the Université Côte d'Azur (ATER). This work was supported by the French government through the UCAJEDI Investments in the Future project managed by the National Research Agency (ANR) with the reference number ANR-15-IDEX-01 and through the ANR-22-CE35-0006-01 (BaDAss) to A.G. This work was supported by CNRS, ANR BACNEURODRO (ANR-17-CE16-0023-01), Equipe Fondation pour la Recherche Médicale (EQU201603007783) and the ANR Pepneuron (ANR-21-CE16-0027) to J.R. and L.K.

928 **REFERENCES**

929 **Arias-Rojas, A., Frahm, D., Hurwitz, R., Brinkmann, V. and Iatsenko, I.** (2023). Resistance to host
930 antimicrobial peptides mediates resilience of gut commensals during infection and aging in Drosophila.
931 *Proc Natl Acad Sci U S A* **120**, e2305649120.
932 **Basset, A., Khush, R. S., Braun, A., Gardan, L., Boccard, F., Hoffmann, J. A. and Lemaitre, B.** (2000).
933 The phytopathogenic bacteria Erwinia carotovora infects Drosophila and activates an immune
934 response. *Proc Natl Acad Sci U S A* **97**, 3376-81.
935 **Bataillé, L., Colombié, N., Pelletier, A., Paululat, A., Lebreton, G., Carrier, Y., Frendo, J. L. and Vincent,**
936 **A.** (2020). Alary muscles and thoracic alary-related muscles are atypical striated muscles involved in
937 maintaining the position of internal organs. *Development* **147**.
938 **Belinskaia, M., Wang, J., Kaza, S. K., Antoniazzi, C., Zurawski, T., Dolly, J. O. and Lawrence, G. W.**
939 (2023). Bipartite Activation of Sensory Neurons by a TRPA1 Agonist Allyl Isothiocyanate Is Reflected by
940 Complex Ca(2+) Influx and CGRP Release Patterns: Enhancement by NGF and Inhibition with VAMP and
941 SNAP-25 Cleaving Botulinum Neurotoxins. *Int J Mol Sci* **24**.
942 **Benguettat, O., Jneid, R., Soltys, J., Loudhaief, R., Brun-Barale, A., Osman, D. and Gallet, A.** (2018).
943 The DH31/CGRP enteroendocrine peptide triggers intestinal contractions favoring the elimination of
944 opportunistic bacteria. *PLoS Pathog.* **14**, e1007279. doi: 10.1371/journal.ppat.1007279. eCollection
945 2018 Sep.
946 **Bosco-Drayon, V., Poidevin, M., Boneca, I. G., Narbonne-Reveau, K., Royet, J. and Charroux, B.**
947 (2012). Peptidoglycan sensing by the receptor PGRP-LE in the Drosophila gut induces immune
948 responses to infectious bacteria and tolerance to microbiota. *Cell Host Microbe* **12**, 153-65.
949 **Bulc, M., Palus, K., Całka, J. and Zielonka, Ł.** (2018). Changes in Immunoreactivity of Sensory
950 Substances within the Enteric Nervous System of the Porcine Stomach during Experimentally Induced
951 Diabetes. *J Diabetes Res* **2018**, 4735659.
952 **Capo, F., Charroux, B. and Royet, J.** (2016). Bacteria sensing mechanisms in Drosophila gut: Local and
953 systemic consequences. *Dev Comp Immunol* **64:11-21.**, 10.1016/j.dci.2016.01.001. Epub 2016 Jan 8.
954 **Carboni, A. L., Hanson, M. A., Lindsay, S. A., Wasserman, S. A. and Lemaitre, B.** (2022). Cecropins
955 contribute to Drosophila host defense against a subset of fungal and Gram-negative bacterial infection.
956 *Genetics* **220**.
957 **Chakrabarti, S., Liehl, P., Buchon, N. and Lemaitre, B.** (2012). Infection-induced host translational
958 blockage inhibits immune responses and epithelial renewal in the Drosophila gut. *Cell Host Microbe*
959 **12**, 60-70. doi: 10.1016/j.chom.2012.06.001.
960 **Chen, J., Kim, S. M. and Kwon, J. Y.** (2016). A Systematic Analysis of Drosophila Regulatory Peptide
961 Expression in Enteroendocrine Cells. 10.14348/molcells.2016.0014.
962 **Dombrovski, M., Kim, A., Poussard, L., Vaccari, A., Acton, S., Spillman, E., Condron, B. and Yuan, Q.**
963 (2019). A Plastic Visual Pathway Regulates Cooperative Behavior in Drosophila Larvae. *Curr Biol* **29**,
964 1866-1876.e5.
965 **Dombrovski, M., Poussard, L., Moalem, K., Kmecova, L., Hogan, N., Schott, E., Vaccari, A., Acton, S.**
966 **and Condron, B.** (2017). Cooperative Behavior Emerges among Drosophila Larvae. *Curr Biol* **27**, 2821-
967 2826.e2.
968 **Du, E. J., Ahn, T. J., Kwon, I., Lee, J. H., Park, J. H., Park, S. H., Kang, T. M., Cho, H., Kim, T. J., Kim, H.**
969 **W. et al.** (2016a). TrpA1 Regulates Defecation of Food-Borne Pathogens under the Control of the Duox
970 Pathway. *PLoS Genet* **12**, e1005773. doi: 10.1371/journal.pgen.1005773. eCollection 2016 Jan.
971 **Du, E. J., Ahn, T. J., Wen, X., Seo, D. W., Na, D. L., Kwon, J. Y., Choi, M., Kim, H. W., Cho, H. and Kang,**
972 **K.** (2016b). Nucleophile sensitivity of Drosophila TRPA1 underlies light-induced feeding deterrence.
973 *Elife* **5**.
974 **Earl, S. C., Rogers, M. T., Keen, J., Bland, D. M., Houppert, A. S., Miller, C., Temple, I., Anderson, D.**
975 **M. and Marketon, M. M.** (2015). Resistance to Innate Immunity Contributes to Colonization of the
976 Insect Gut by Yersinia pestis. *PLoS One* **10**, e0133318.

Gu, P., Gong, J., Shang, Y., Wang, F., Ruppell, K. T., Ma, Z., Sheehan, A. E., Freeman, M. R. and Xiang, Y. (2019). Polymodal Nociception in Drosophila Requires Alternative Splicing of TrpA1. *Curr Biol* **29**, 3961-3973.e6.

Guntur, A. R., Gu, P., Takle, K., Chen, J., Xiang, Y. and Yang, C. H. (2015). Drosophila TRPA1 isoforms detect UV light via photochemical production of H2O2. *Proc Natl Acad Sci U S A* **112**, E5753-61.

Guo, X., Lv, J. and Xi, R. (2021). The specification and function of enteroendocrine cells in Drosophila and mammals: a comparative review. *Febs j*.

Ha, E. M., Lee, K. A., Seo, Y. Y., Kim, S. H., Lim, J. H., Oh, B. H., Kim, J. and Lee, W. J. (2009). Coordination of multiple dual oxidase-regulatory pathways in responses to commensal and infectious microbes in drosophila gut. *Nat Immunol* **10**, 949-57. doi: 10.1038/ni.1765. Epub 2009 Aug 9.

Ha, E. M., Oh, C. T., Bae, Y. S. and Lee, W. J. (2005). A direct role for dual oxidase in Drosophila gut immunity. *Science* **310**, 847-50.

Hachfi, S., Brun-Barale, A., Munro, P., Nawrot-Esposito, M.-P., Michel, G., Fichant, A., Bonis, M., Ruimy, R., Boyer, L. and Gallet, A. (2023). Ingestion of Bacillus cereus spores dampens the immune response to favor bacterial persistence. *bioRxiv*.

Hanson, M. A. and Lemaitre, B. (2020). New insights on Drosophila antimicrobial peptide function in host defense and beyond. *Curr Opin Immunol* **62**, 22-30.

Hegedus, D., Erlandson, M., Gillott, C. and Toprak, U. (2009). New insights into peritrophic matrix synthesis, architecture, and function. *Annu Rev Entomol* **54**, 285-302.

Kaneko, T., Yano, T., Aggarwal, K., Lim, J. H., Ueda, K., Oshima, Y., Peach, C., Erturk-Hasdemir, D., Goldman, W. E., Oh, B. H. et al. (2006). PGRP-LC and PGRP-LE have essential yet distinct functions in the drosophila immune response to monomeric DAP-type peptidoglycan. *Nat Immunol* **7**, 715-23.

Kasacka, I. (2009). Quantitative distribution and localization of calcitonin gene-related peptide-like cells in the stomach of two kidney, one clip rats. *J Physiol Pharmacol* **60**, 35-9.

Keita, S., Masuzzo, A., Royet, J. and Kurz, C. L. (2017). Drosophila larvae food intake cessation following exposure to Erwinia contaminated media requires odor perception, Trpa1 channel and evf virulence factor. *J Insect Physiol.* **99:25-32.**, 10.1016/j.jinsphys.2017.02.004. Epub 2017 Feb 21.

Kondo, T., Oshima, T., Obata, K., Sakurai, J., Knowles, C. H., Matsumoto, T., Noguchi, K. and Miwa, H. (2010). Role of transient receptor potential A1 in gastric nociception. *Digestion* **82**, 150-5.

Kunst, M., Hughes, M. E., Raccuglia, D., Felix, M., Li, M., Barnett, G., Duah, J. and Nitabach, M. N. (2014). Calcitonin gene-related peptide neurons mediate sleep-specific circadian output in Drosophila. *Curr Biol* **24**, 2652-64.

LaJeunesse, D. R., Johnson, B., Presnell, J. S., Catignas, K. K. and Zapotoczny, G. (2010). Peristalsis in the junction region of the Drosophila larval midgut is modulated by DH31 expressing enteroendocrine cells. *BMC Physiol* **10:14.**, 10.1186/1472-6793-10-14.

Lapointe, T. K. and Altier, C. (2011). The role of TRPA1 in visceral inflammation and pain. *Channels* **5**, 525-9. doi: 10.4161/chan.5.6.18016. Epub 2011 Nov 1.

Lee, K. A., Kim, S. H., Kim, E. K., Ha, E. M., You, H., Kim, B., Kim, M. J., Kwon, Y., Ryu, J. H. and Lee, W. J. (2013). Bacterial-derived uracil as a modulator of mucosal immunity and gut-microbe homeostasis in Drosophila. *Cell* **153**, 797-811. doi: 10.1016/j.cell.2013.04.009.

Lemaitre, B. and Miguel-Aliaga, I. (2013). The digestive tract of Drosophila melanogaster. *Annu Rev Genet* **47:377-404.**, 10.1146/annurev-genet-111212-133343.

Leulier, F., Parquet, C., Pili-Floury, S., Ryu, J. H., Caroff, M., Lee, W. J., Mengin-Lecreulx, D. and Lemaitre, B. (2003). The Drosophila immune system detects bacteria through specific peptidoglycan recognition. *Nat Immunol* **4**, 478-84.

Liehl, P., Blight, M., Vodovar, N., Boccard, F. and Lemaitre, B. (2006). Prevalence of local immune response against oral infection in a Drosophila/Pseudomonas infection model. *PLoS Pathog.* **2**, e56. doi: 10.1371/journal.ppat.0020056. Epub 2006 Jun 9.

Loudhaief, R., Brun-Barale, A., Benguettat, O., Nawrot-Esposito, M. P., Pauron, D., Amichot, M. and Gallet, A. (2017). Apoptosis restores cellular density by eliminating a physiologically or genetically induced excess of enterocytes in the Drosophila midgut. *Development* **144**, 808-819. doi: 10.1242/dev.142539.

Louis, M. and de Polavieja, G. (2017). Collective Behavior: Social Digging in Drosophila Larvae. *Curr Biol* **27**, R1010-r1012.

Mast, J. D., De Moraes, C. M., Alborn, H. T., Lavis, L. D. and Stern, D. L. (2014). Evolved differences in larval social behavior mediated by novel pheromones. *Elife* **3**, e04205.

Nässel, D. R. and Zandawala, M. (2019). Recent advances in neuropeptide signaling in Drosophila, from genes to physiology and behavior. *Prog Neurobiol* **179**, 101607.

Nawrot-Esposito, M. P., Babin, A., Pasco, M., Poirié, M., Gatti, J. L. and Gallet, A. (2020). Bacillus thuringiensis Bioinsecticides Induce Developmental Defects in Non-Target Drosophila melanogaster Larvae. *Insects* **11**.

Neyen, C., Bretscher, A. J., Binggeli, O. and Lemaitre, B. (2014). Methods to study Drosophila immunity. *Methods* **68**, 116-28. doi: 10.1016/j.ymeth.2014.02.023. Epub 2014 Mar 12.

Ogawa, N., Kurokawa, T. and Mori, Y. (2016). Sensing of redox status by TRP channels. *Cell Calcium* **60**, 115-22. doi: 10.1016/j.ceca.2016.02.009. Epub 2016 Mar 4.

Park, D., Veenstra, J. A., Park, J. H. and Taghert, P. H. (2008). Mapping peptidergic cells in Drosophila: where DIMM fits in. *PLoS One.* **3**, e1896. doi: 10.1371/journal.pone.0001896.

Pelaseyed, T., Bergstrom, J. H., Gustafsson, J. K., Ermund, A., Birchenough, G. M., Schutte, A., van der Post, S., Svensson, F., Rodriguez-Pineiro, A. M., Nystrom, E. E. et al. (2014). The mucus and mucins of the goblet cells and enterocytes provide the first defense line of the gastrointestinal tract and interact with the immune system. *Immunol Rev* **260**, 8-20. doi: 10.1111/imr.12182.

Ramond, E., Jamet, A., Ding, X., Euphrasie, D., Bouvier, C., Lallemant, L., He, X., Arbibe, L., Coureuil, M. and Charbit, A. (2021). Reactive Oxygen Species-Dependent Innate Immune Mechanisms Control Methicillin-Resistant Staphylococcus aureus Virulence in the Drosophila Larval Model. *MBio* **12**, e0027621.

Ryu, J. H., Ha, E. M., Oh, C. T., Seol, J. H., Brey, P. T., Jin, I., Lee, D. G., Kim, J., Lee, D. and Lee, W. J. (2006). An essential complementary role of NF-kappaB pathway to microbicidal oxidants in Drosophila gut immunity. *EMBO J* **25**, 3693-701. Epub 2006 Jul 20.

Stenbak, C. R., Ryu, J. H., Leulier, F., Pili-Floury, S., Parquet, C., Hervé, M., Chaput, C., Boneca, I. G., Lee, W. J., Lemaitre, B. et al. (2004). Peptidoglycan molecular requirements allowing detection by the Drosophila immune deficiency pathway. *J Immunol* **173**, 7339-48.

Storelli, G., Strigini, M., Grenier, T., Bozonnet, L., Schwarzer, M., Daniel, C., Matos, R. and Leulier, F. (2018). Drosophila Perpetuates Nutritional Mutualism by Promoting the Fitness of Its Intestinal Symbiont Lactobacillus plantarum. *Cell Metab.* **27**, 362-377.e8. doi: 10.1016/j.cmet.2017.11.011. Epub 2017 Dec 28.

Surendran, S., Huckesfeld, S., Waschle, B. and Pankratz, M. J. (2017). Pathogen-induced food evasion behavior in Drosophila larvae. *J Exp Biol.* **220**, 1774-1780. doi: 10.1242/jeb.153395. Epub 2017 Mar 2.

Veenstra, J. A., Agricola, H. J. and Sellami, A. (2008). Regulatory peptides in fruit fly midgut. *Cell Tissue Res* **334**, 499-516. doi: 10.1007/s00441-008-0708-3. Epub 2008 Oct 30.

Vodovar, N., Vinals, M., Liehl, P., Basset, A., Degrouard, J., Spellman, P., Boccard, F. and Lemaitre, B. (2005). Drosophila host defense after oral infection by an entomopathogenic Pseudomonas species. *Proc Natl Acad Sci U S A* **102**, 11414-9. Epub 2005 Aug 1.

Wu, S. C., Liao, C. W., Pan, R. L. and Juang, J. L. (2012). Infection-induced intestinal oxidative stress triggers organ-to-organ immunological communication in Drosophila. *Cell Host Microbe.* **11**, 410-7. doi: 10.1016/j.chom.2012.03.004.

Younes, S., Al-Sulaiti, A., Nasser, E. A. A., Najjar, H. and Kamareddine, L. (2020). Drosophila as a Model Organism in Host-Pathogen Interaction Studies. *Front Cell Infect Microbiol* **10**, 214.

Zhai, Z., Huang, X. and Yin, Y. (2018). Beyond immunity: The Imd pathway as a coordinator of host defense, organismal physiology and behavior. *Dev Comp Immunol* **83**, 51-59.

FIGURE 1

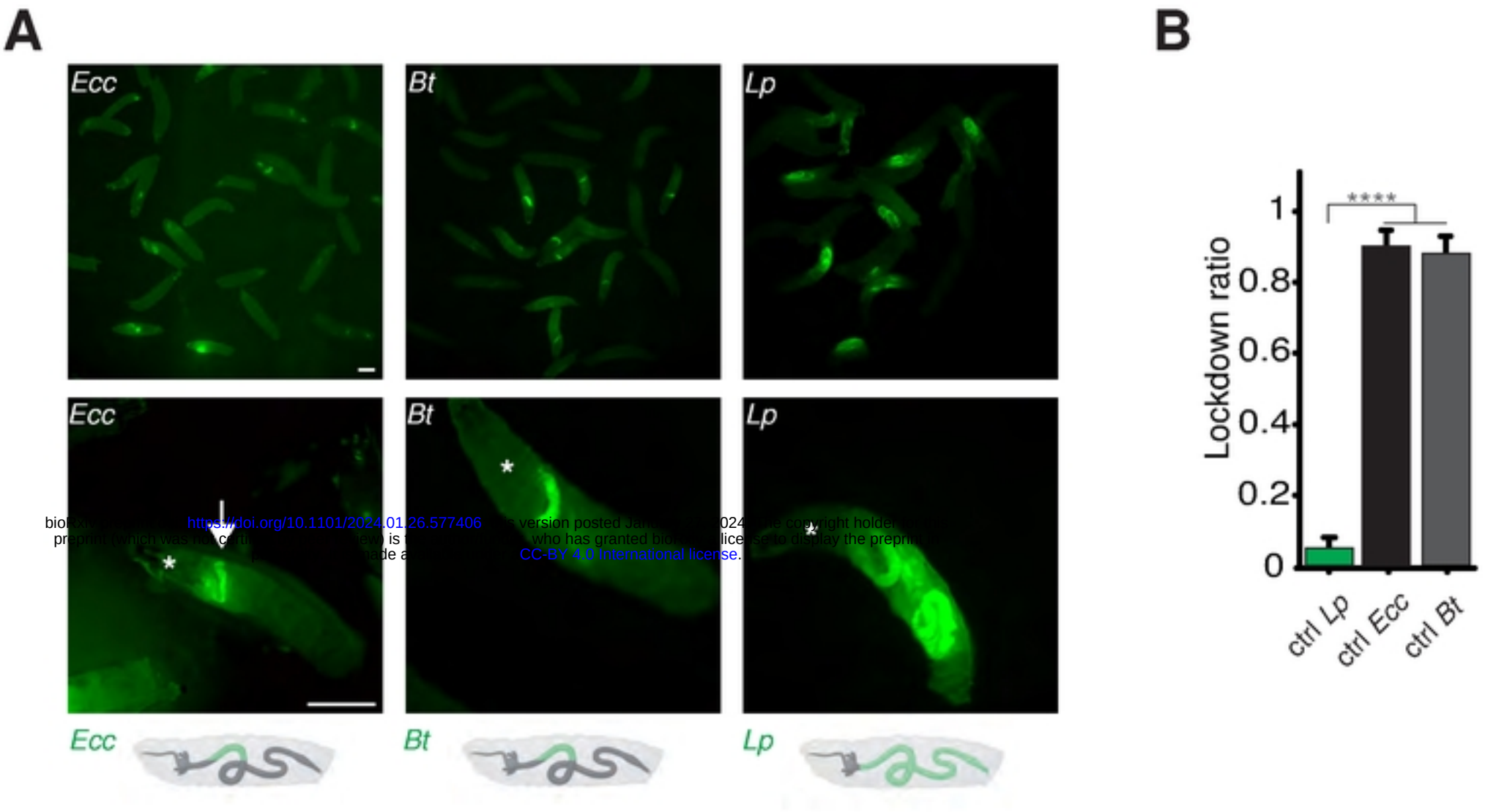

FIGURE 2

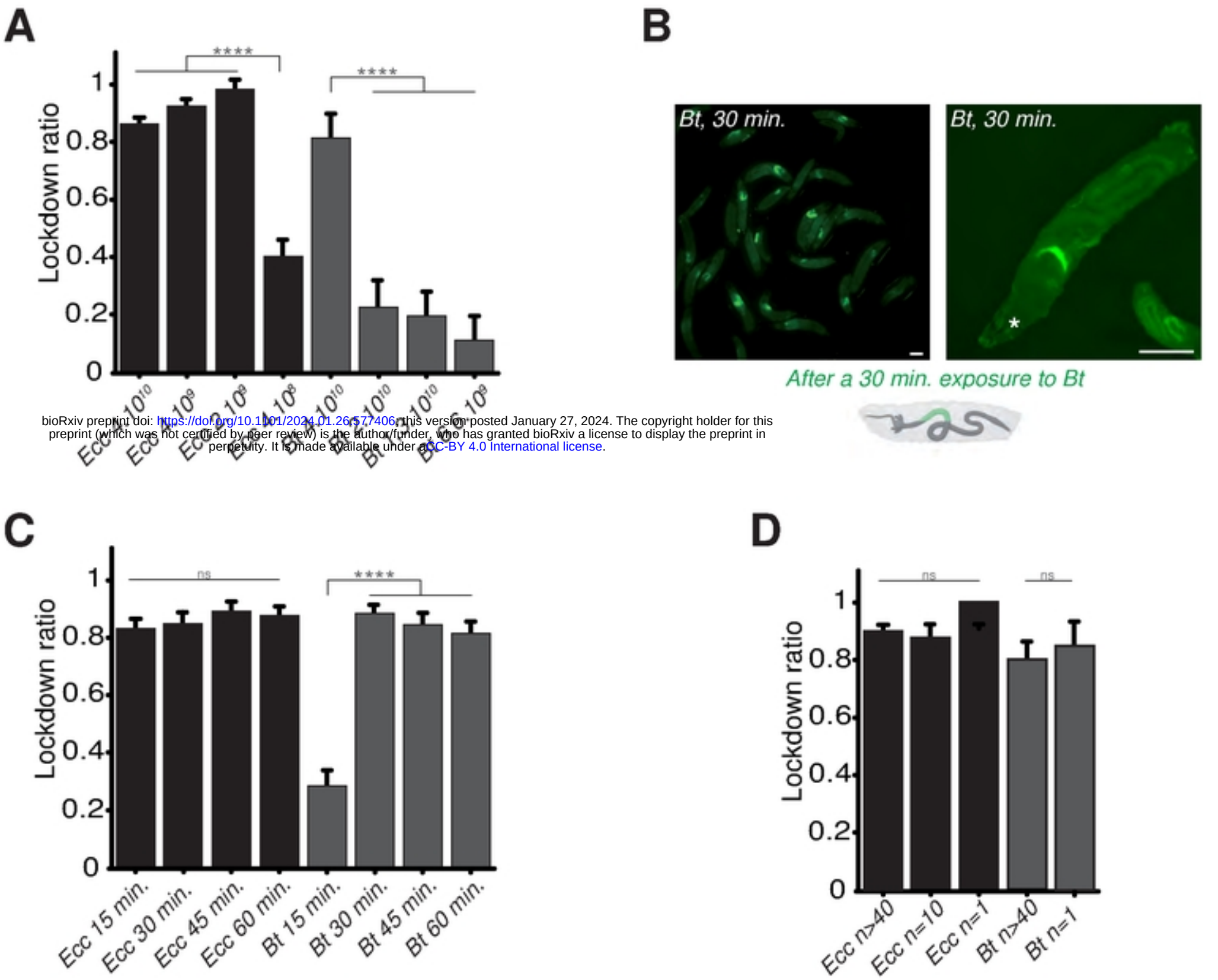

FIGURE 3

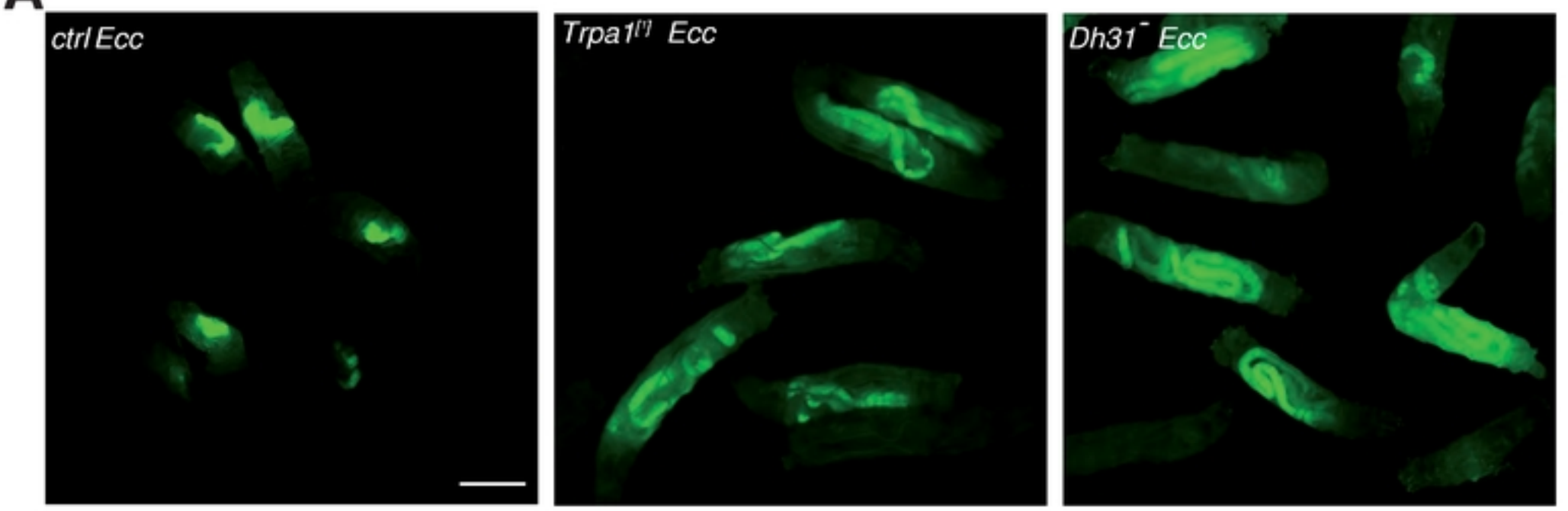

FIGURE 4

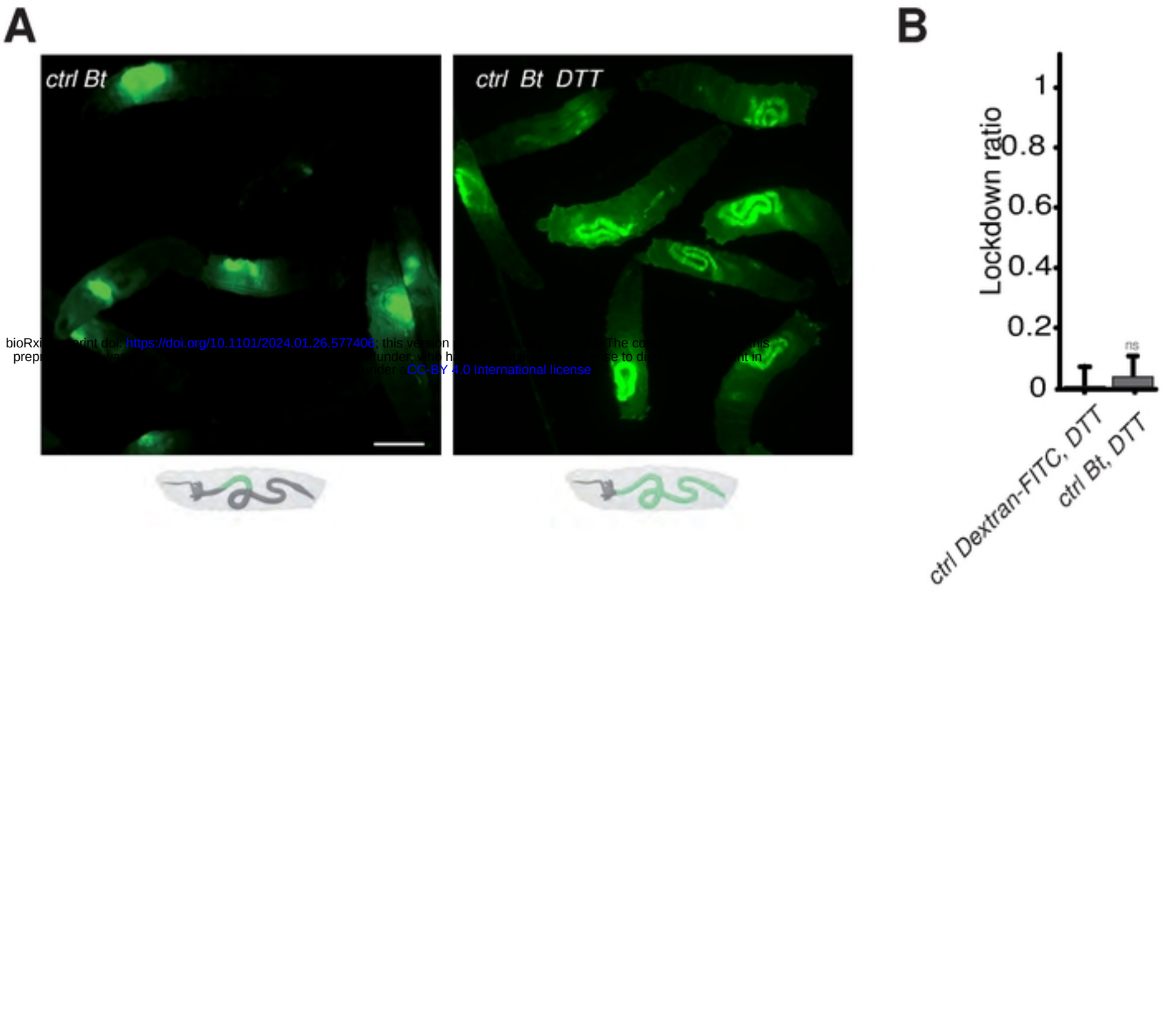

FIGURE 5

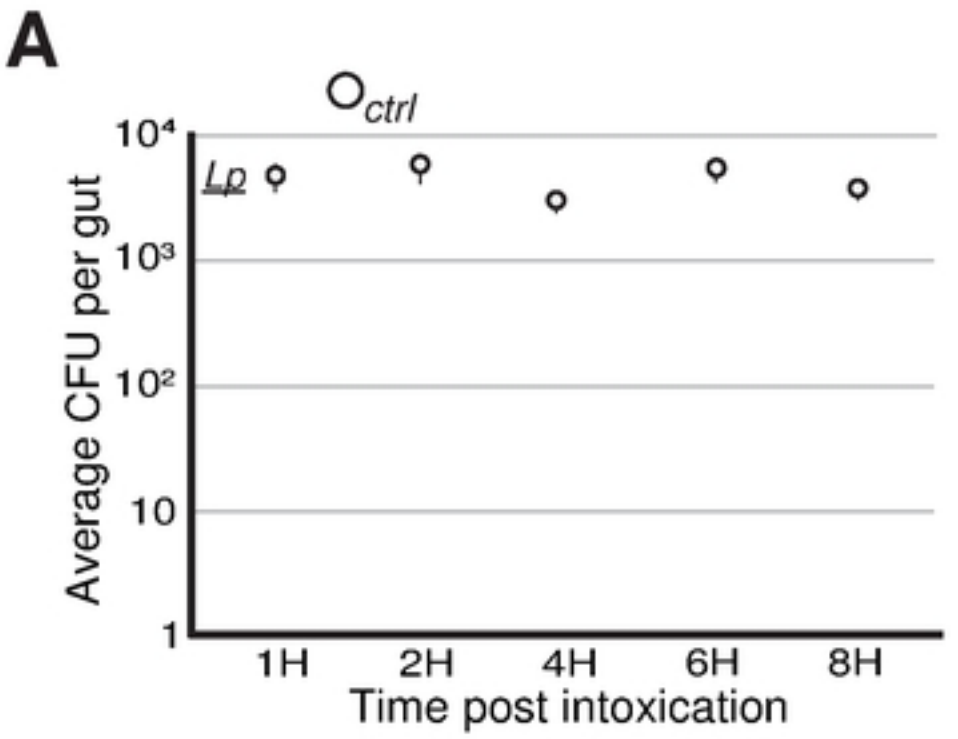

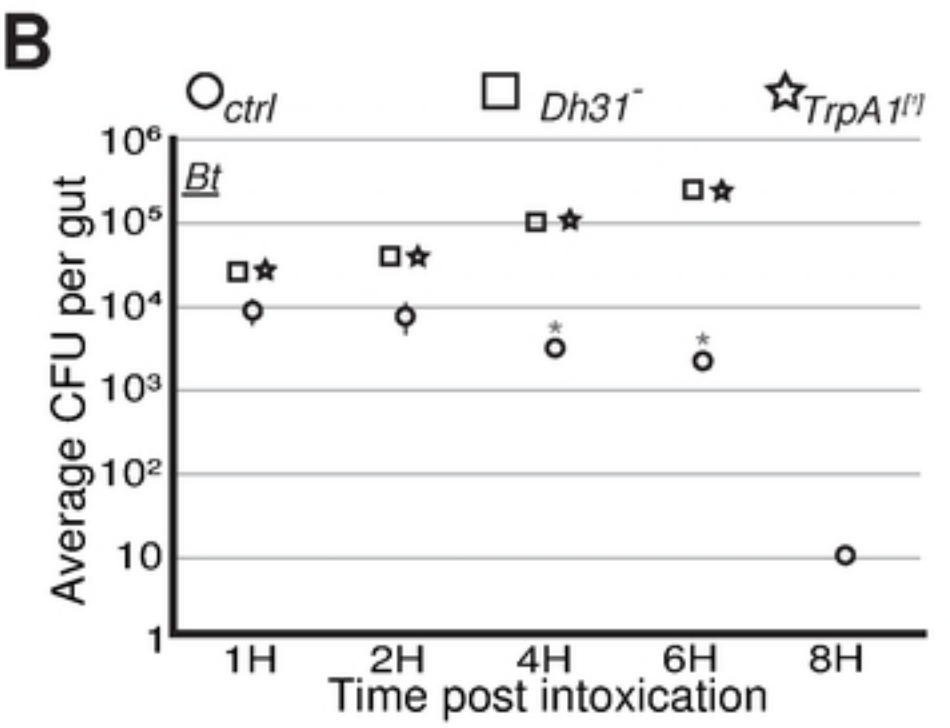

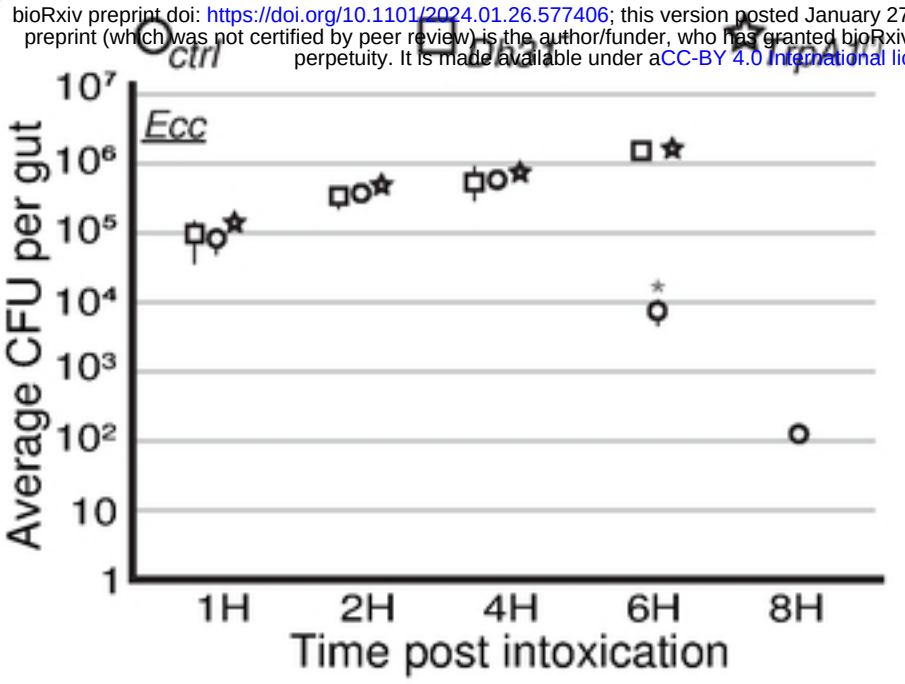

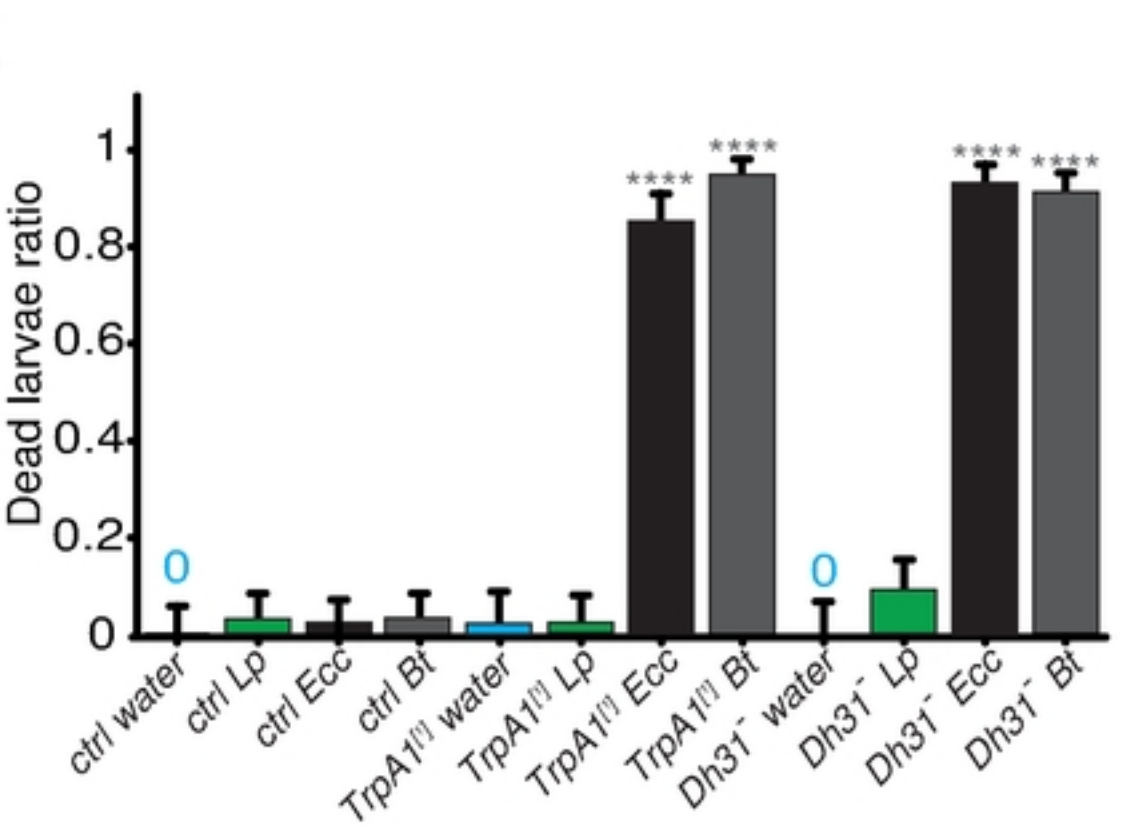

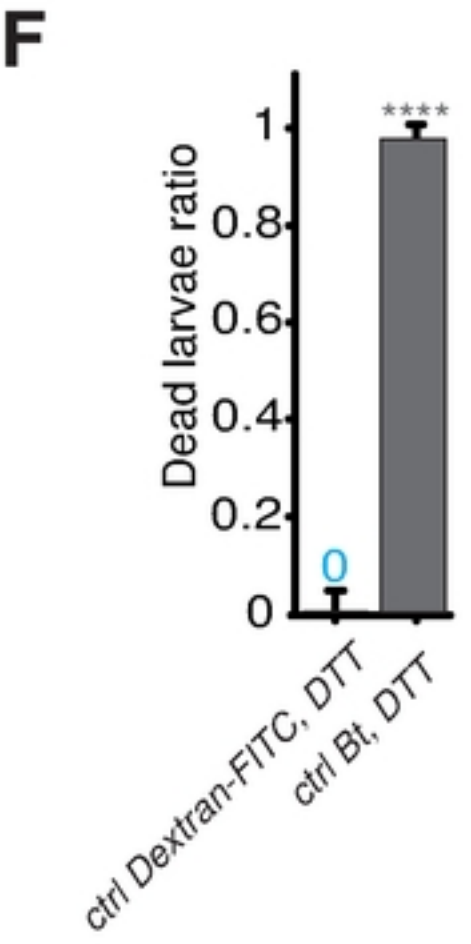

FIGURE 6

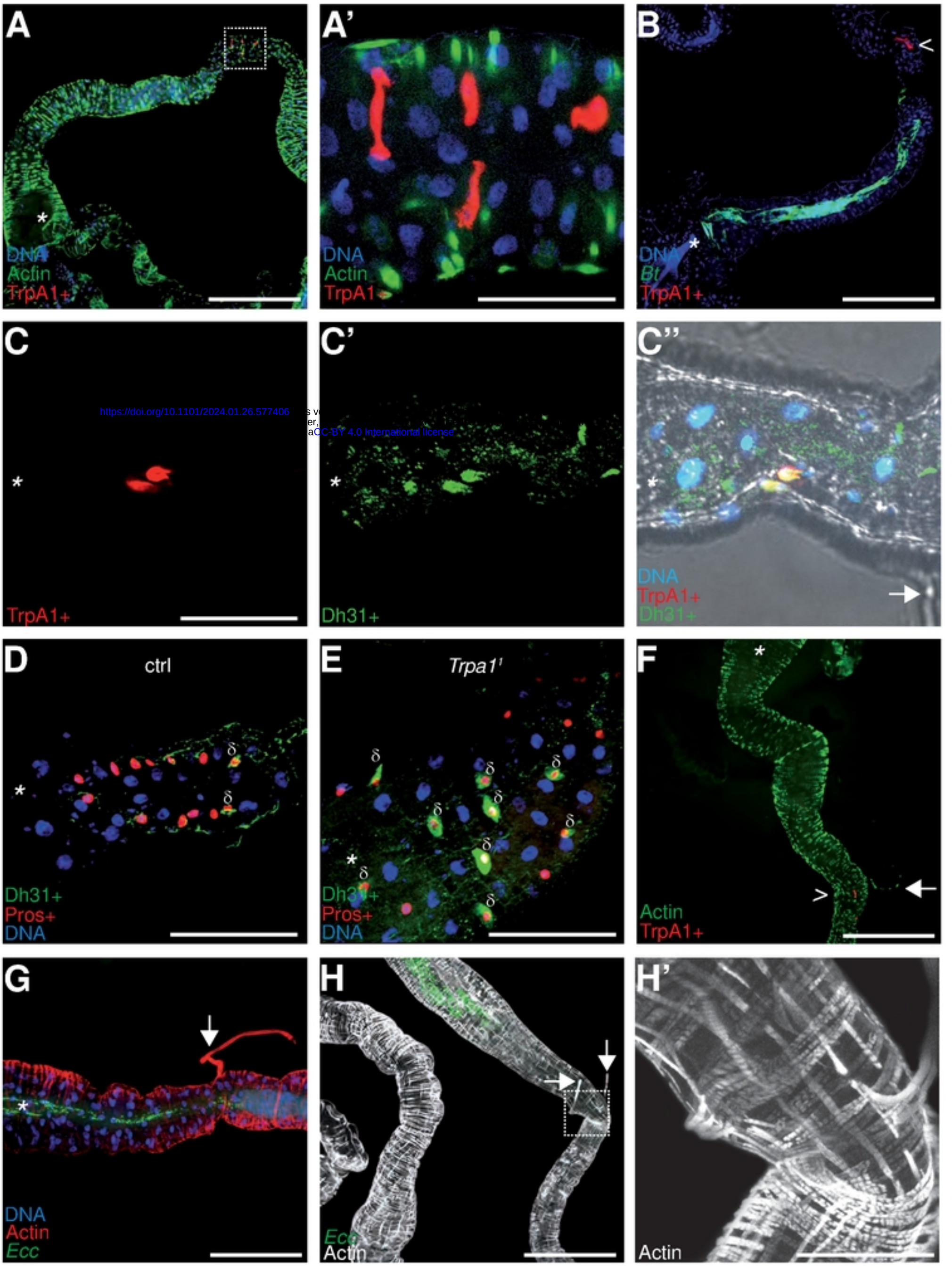

FIGURE 7

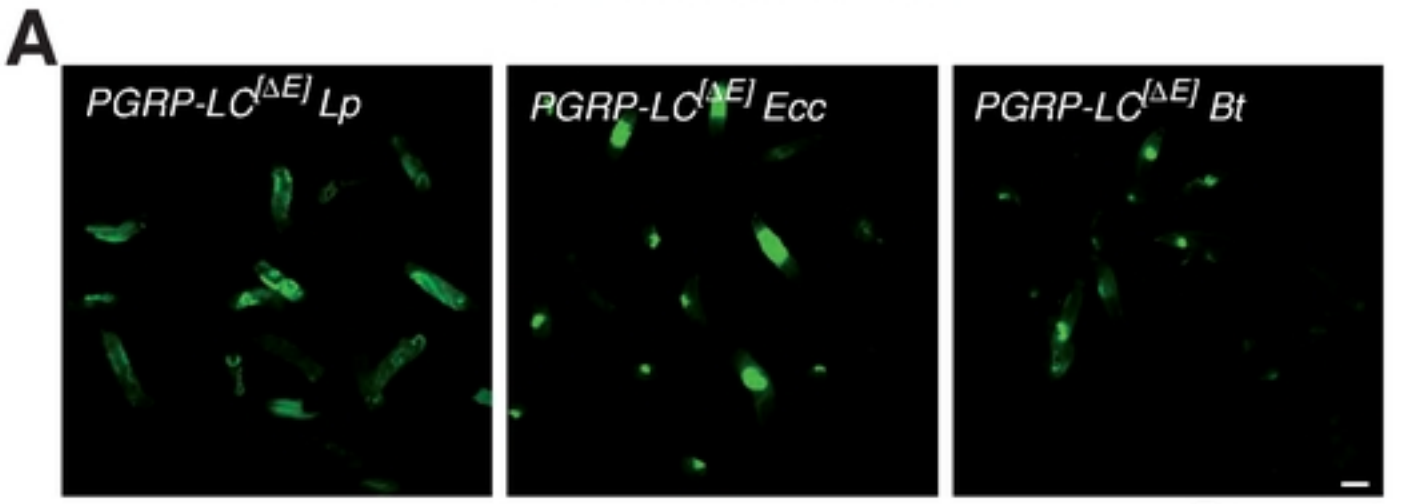

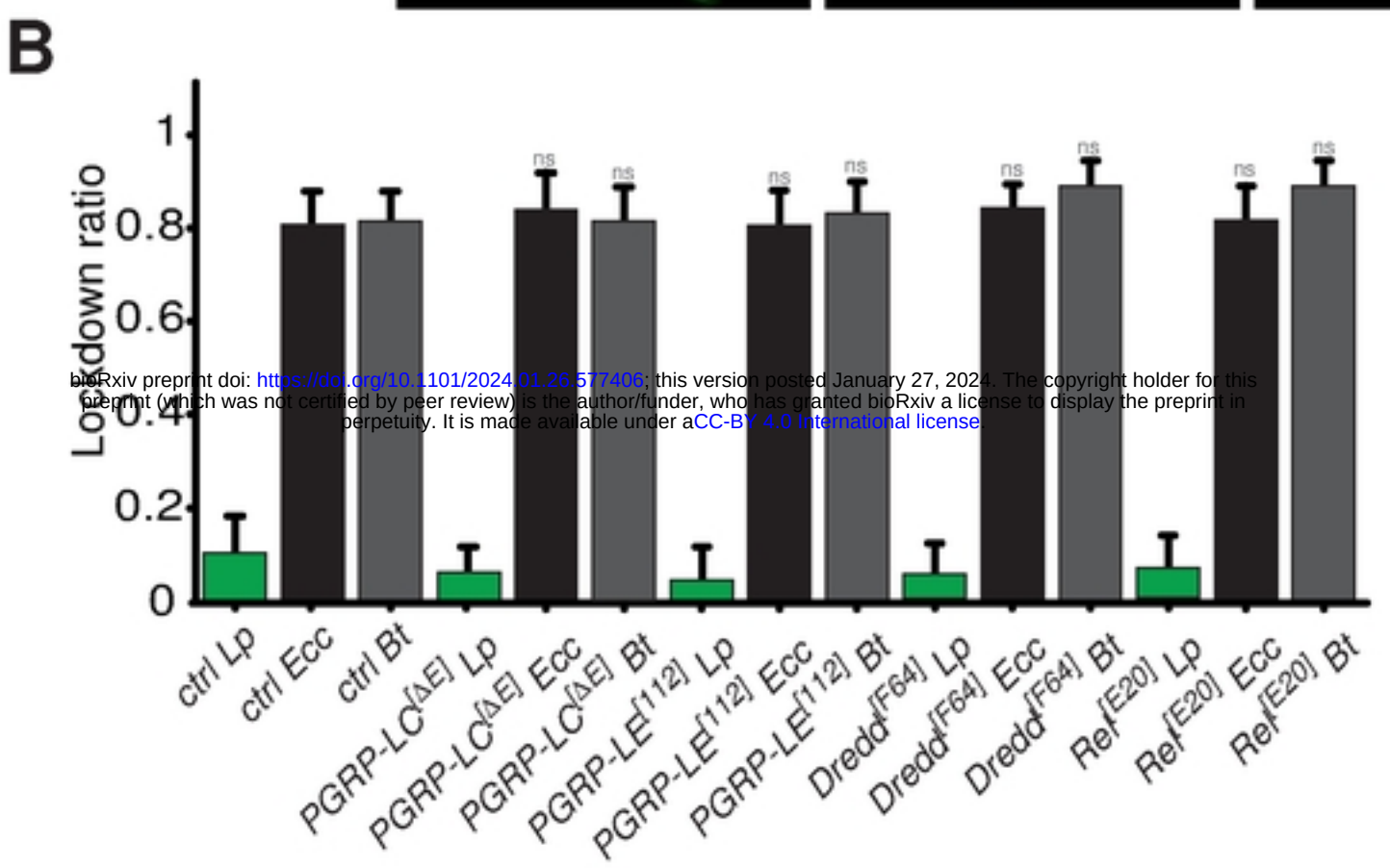

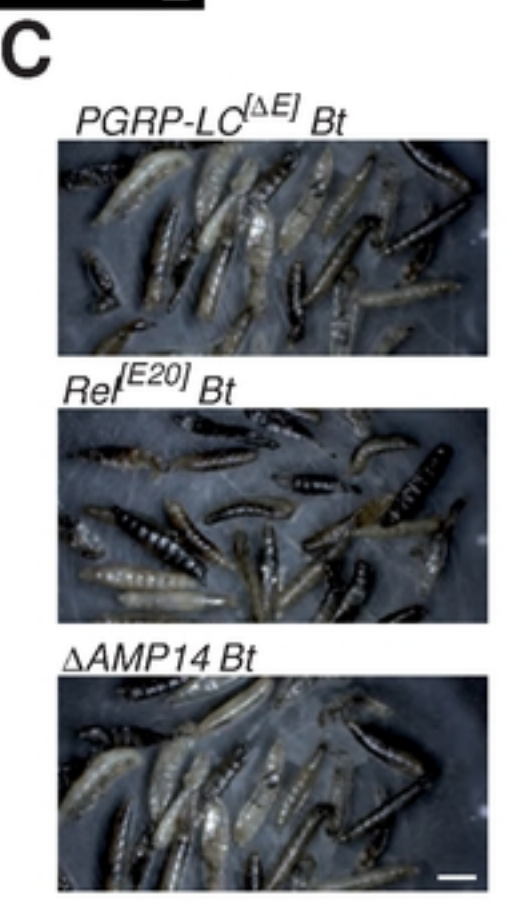

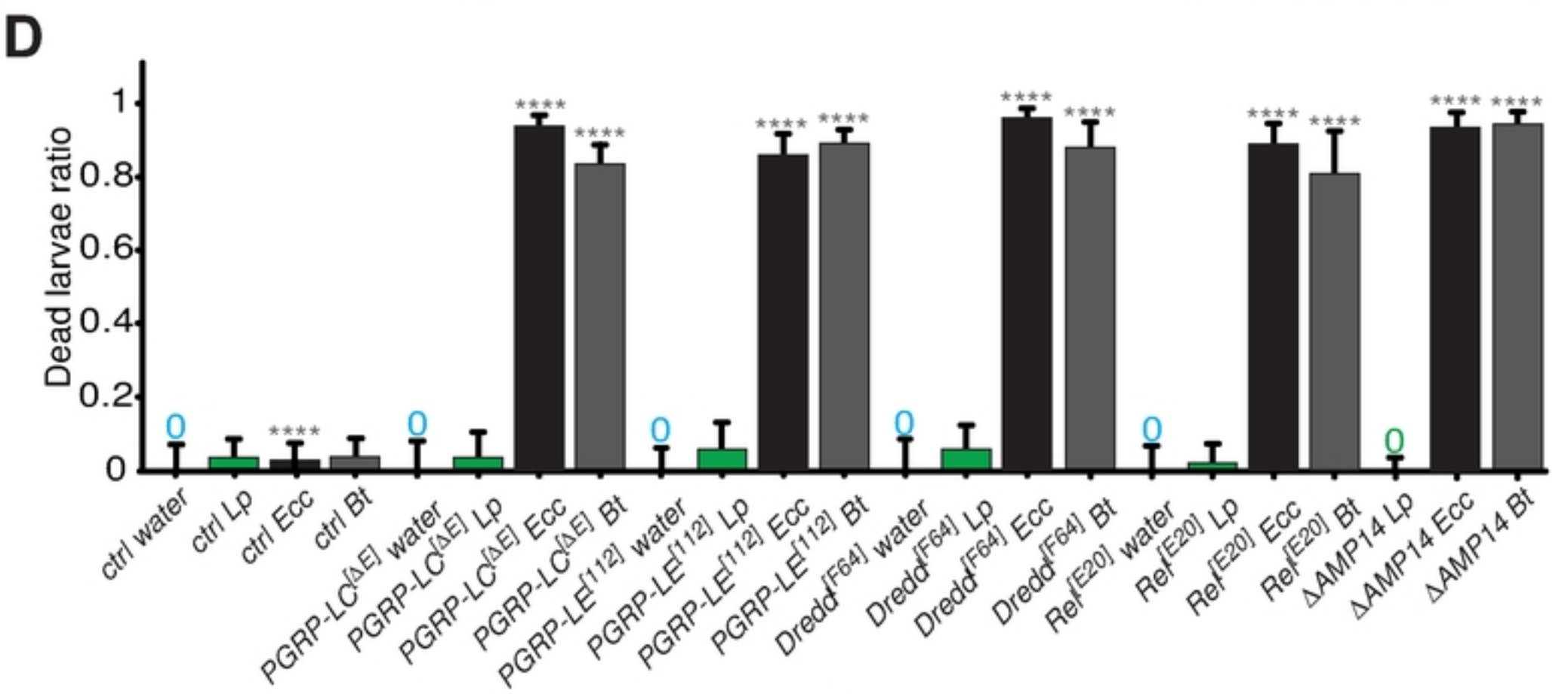

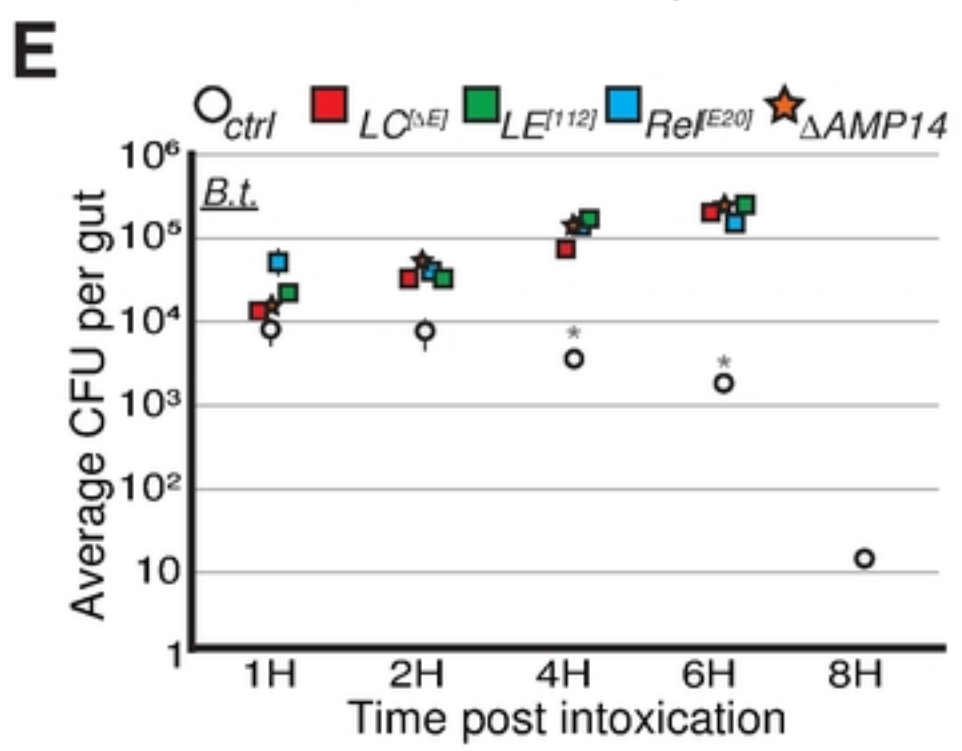

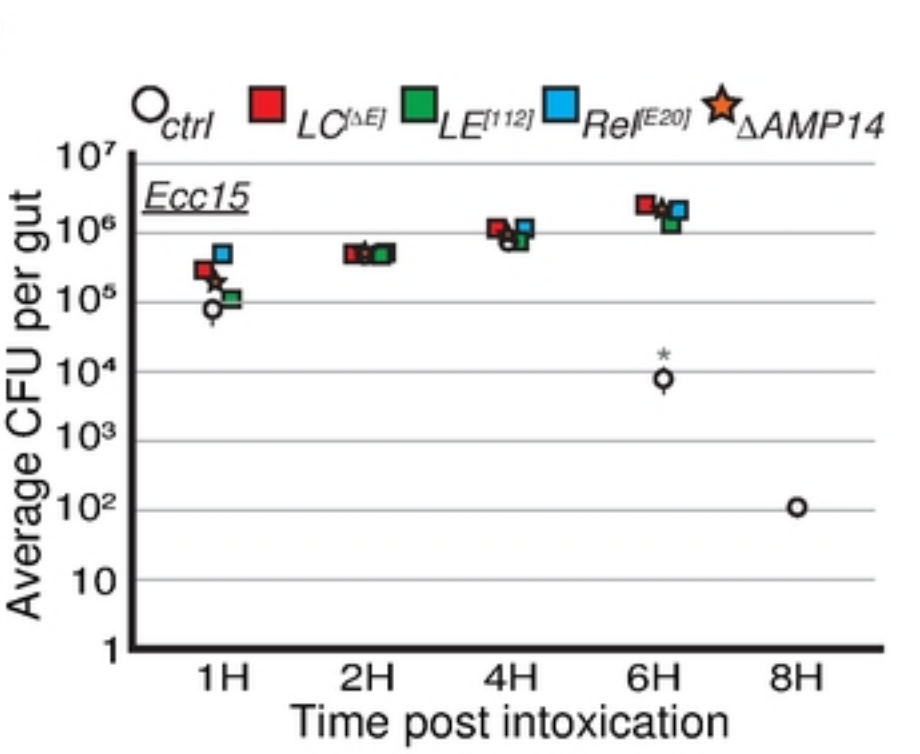

FIGURE 8

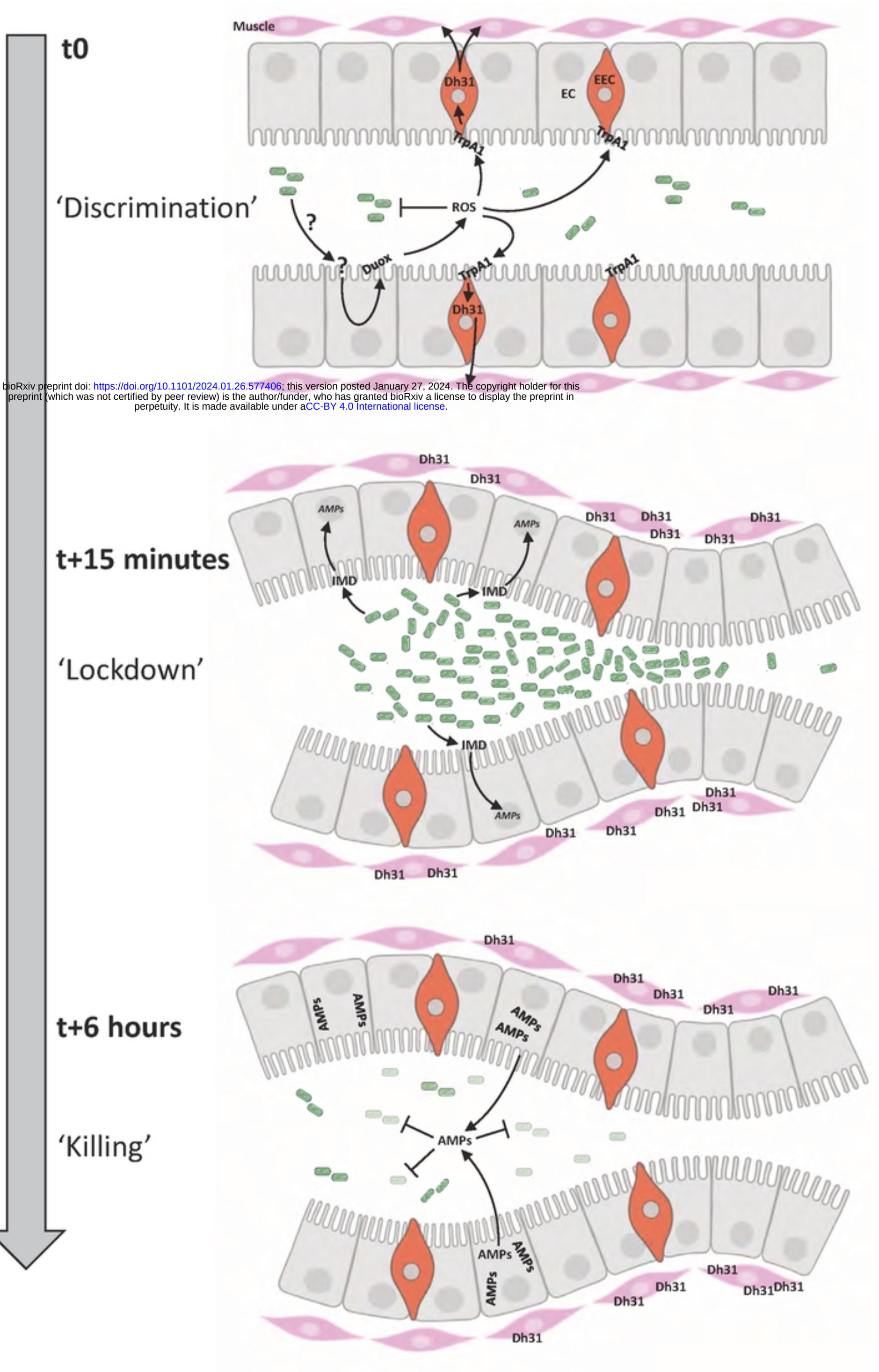

SUPP1

A

ctrl + *Ecc*

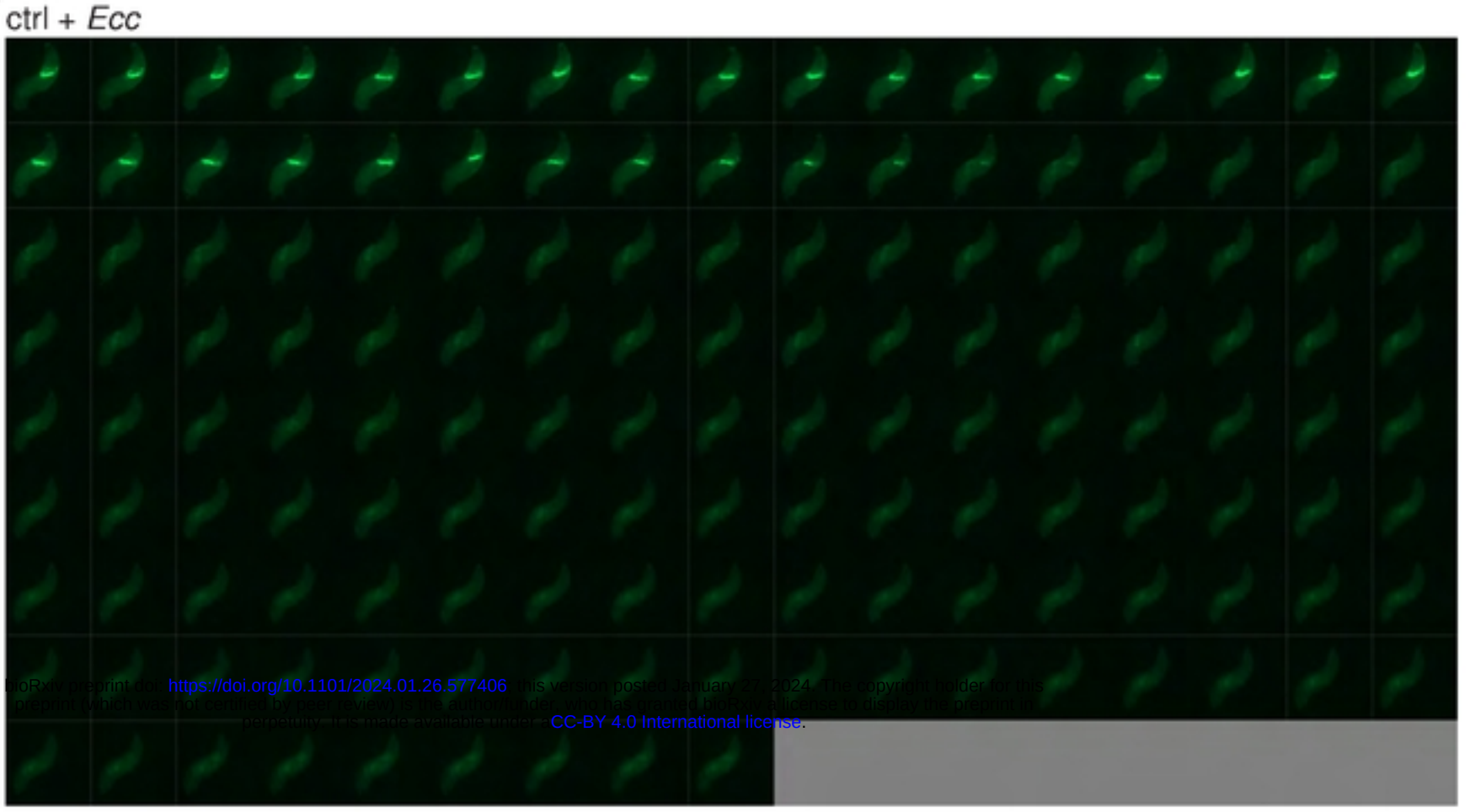

B

ctrl + *Bt*

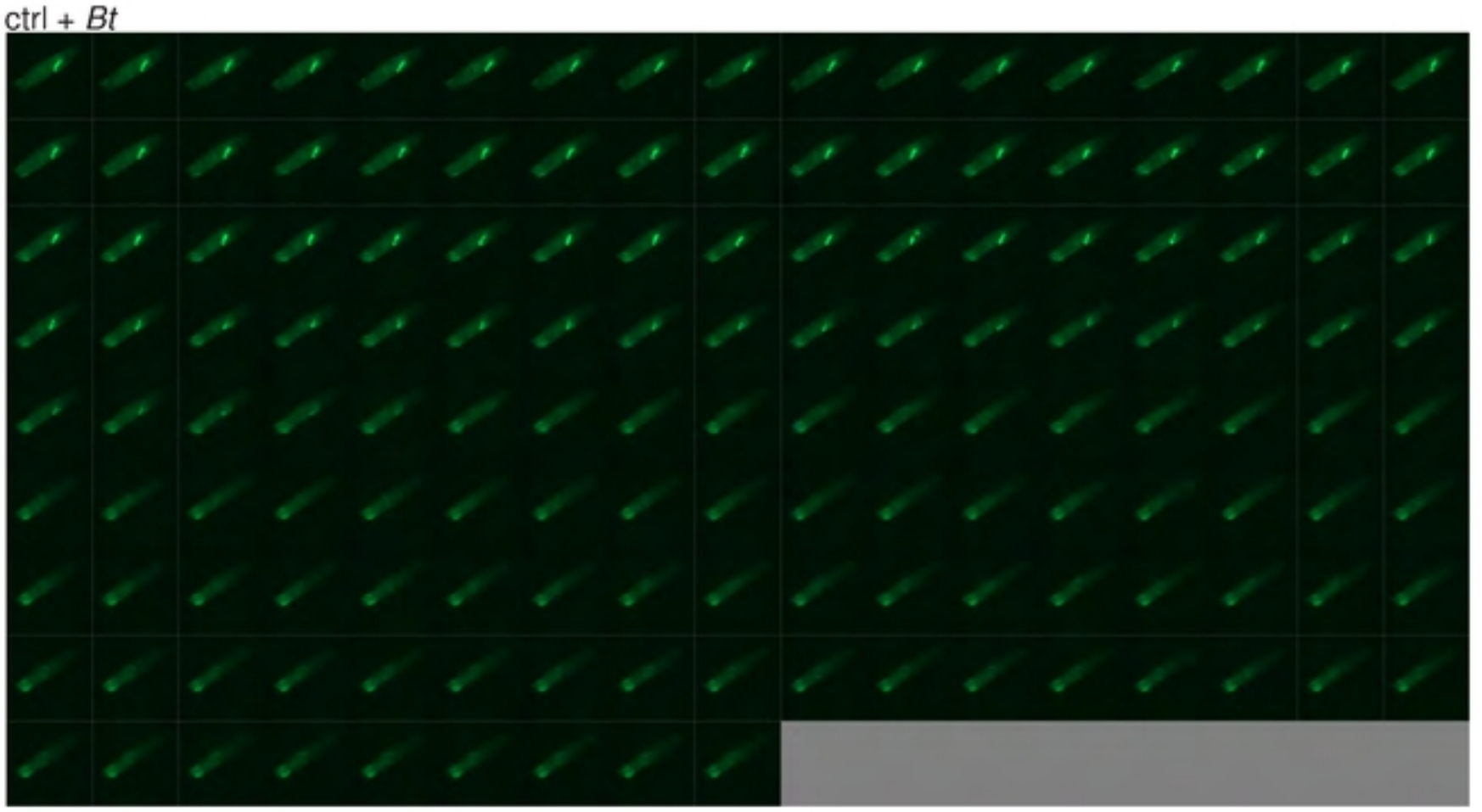

C

ctrl + *Lp*

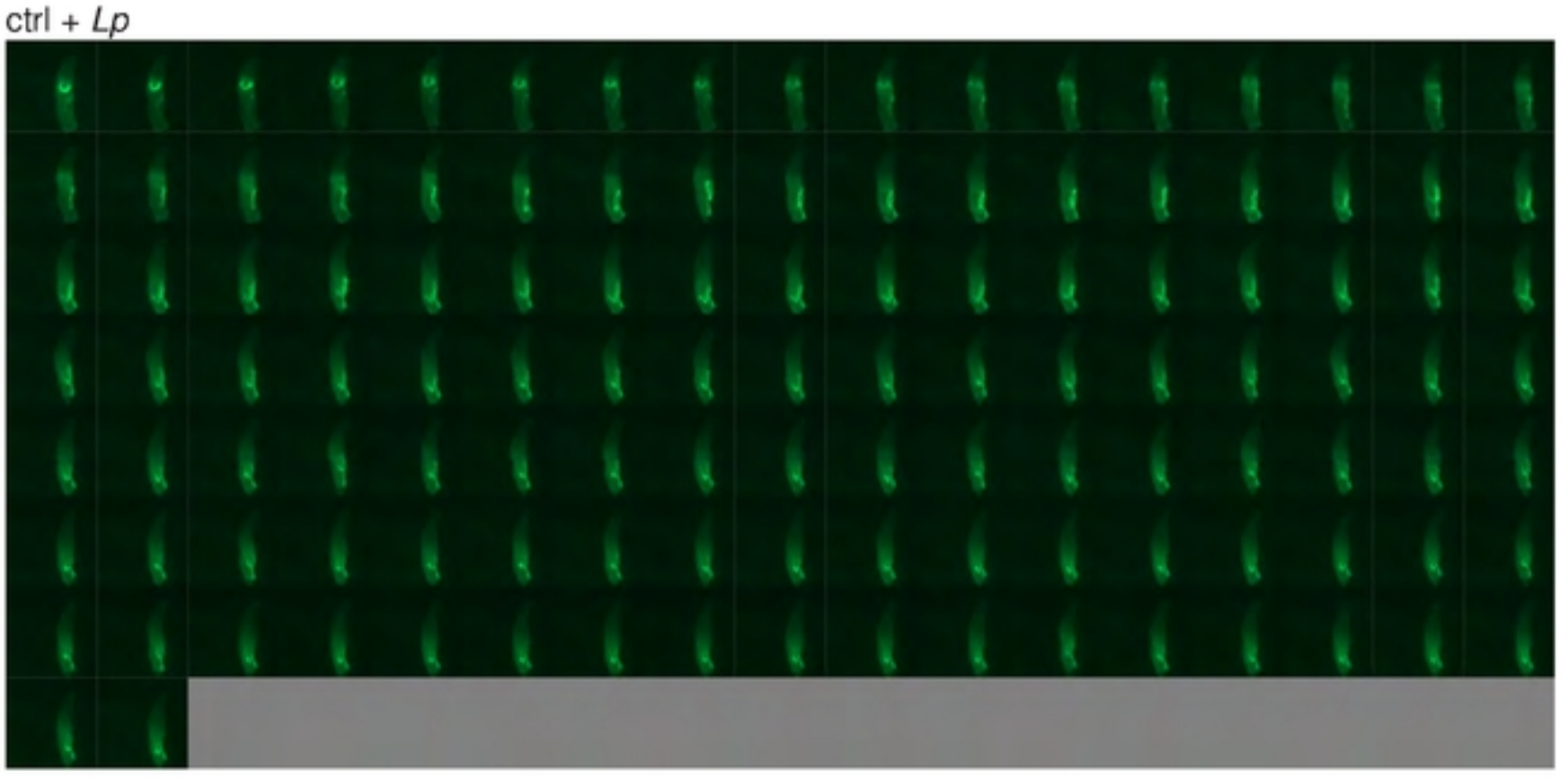

SUPP2

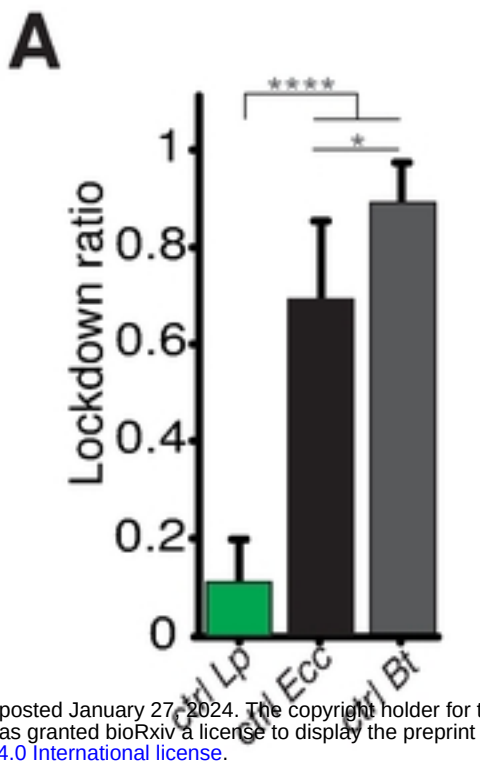

SUPP3

A

TrpA1$^{[1]}$ + *Ecc*

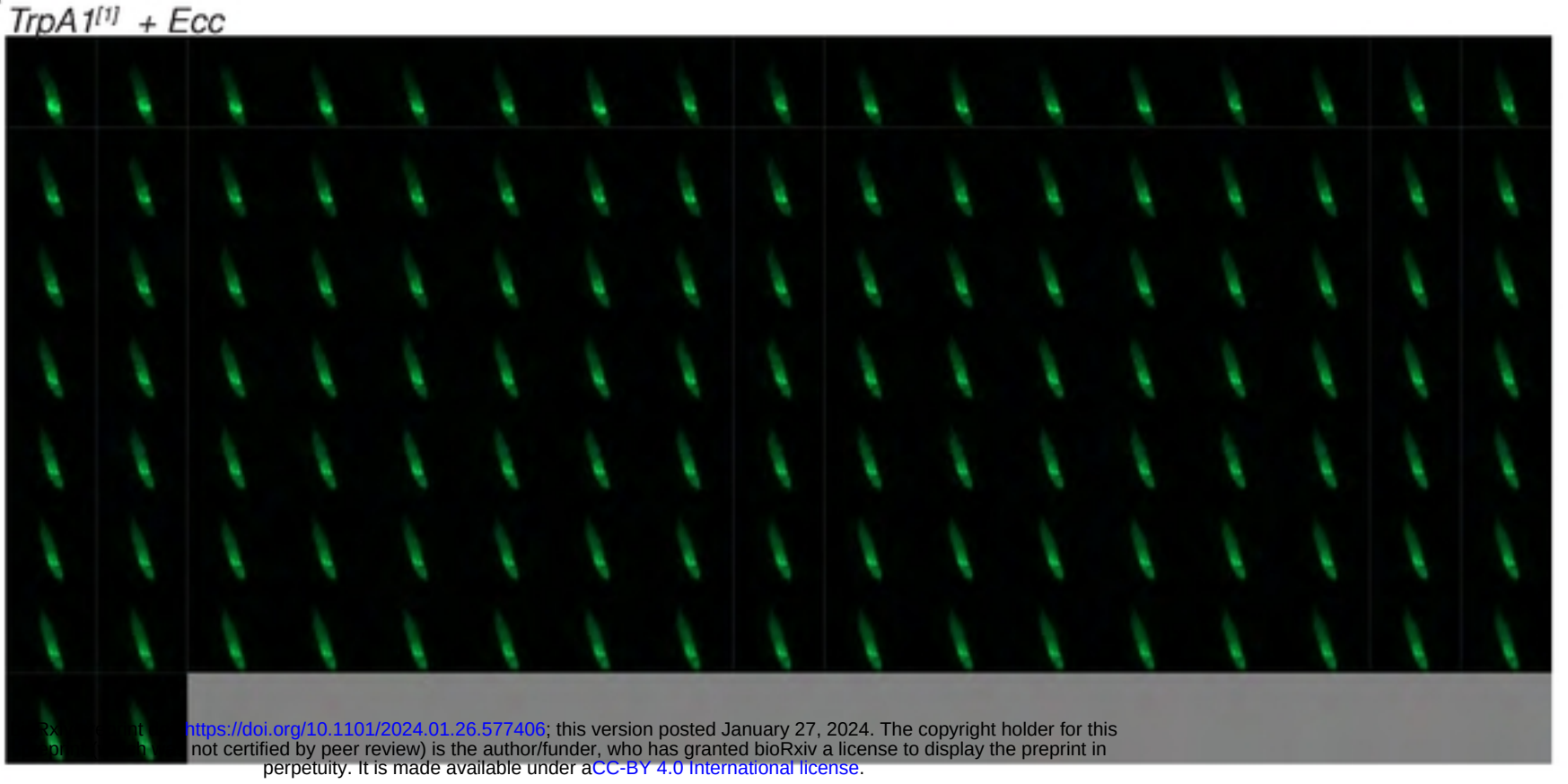

B

Dh31^{-} + *Ecc*

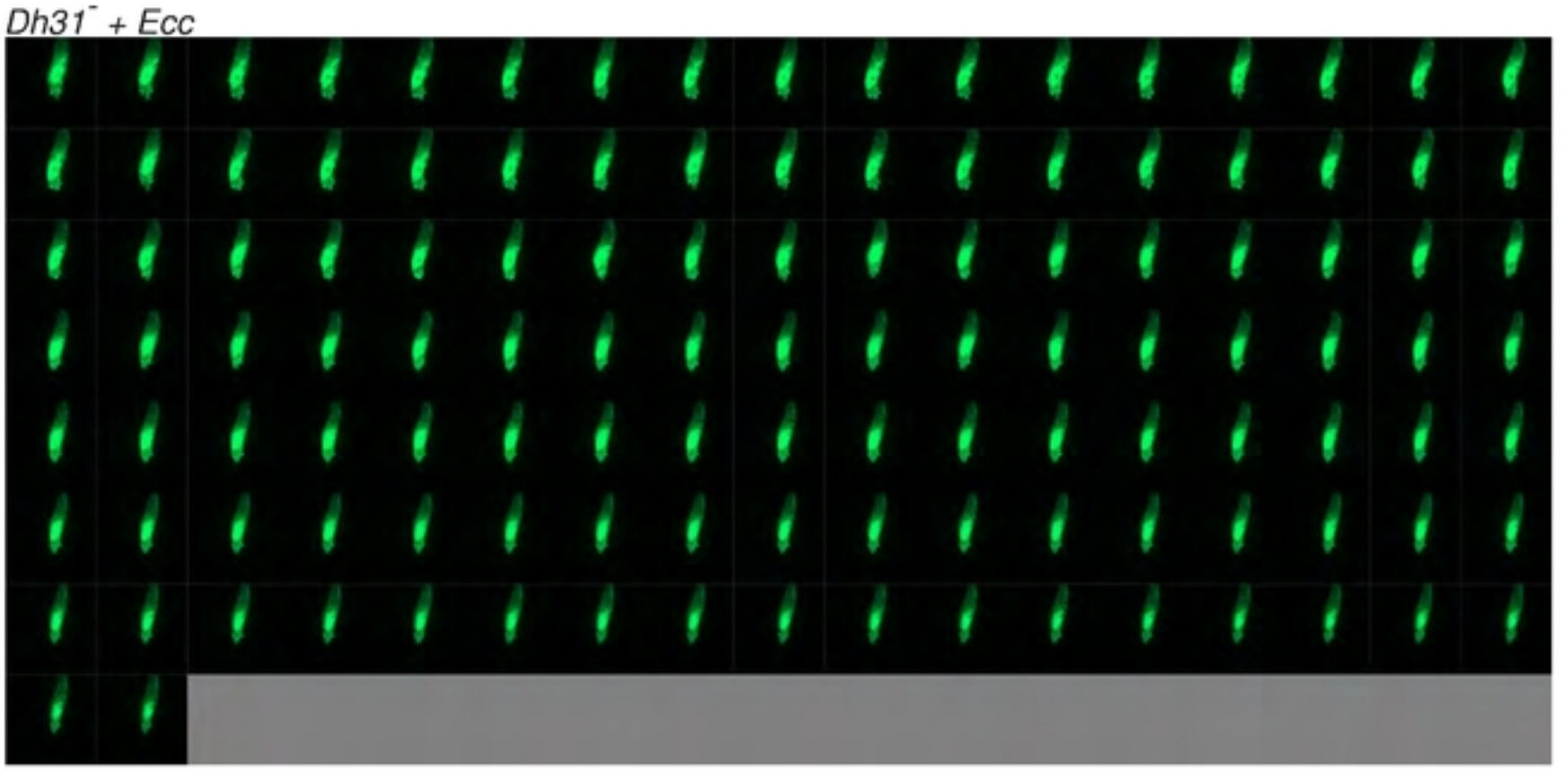

C

ctrl + *Lp* + hCGRP

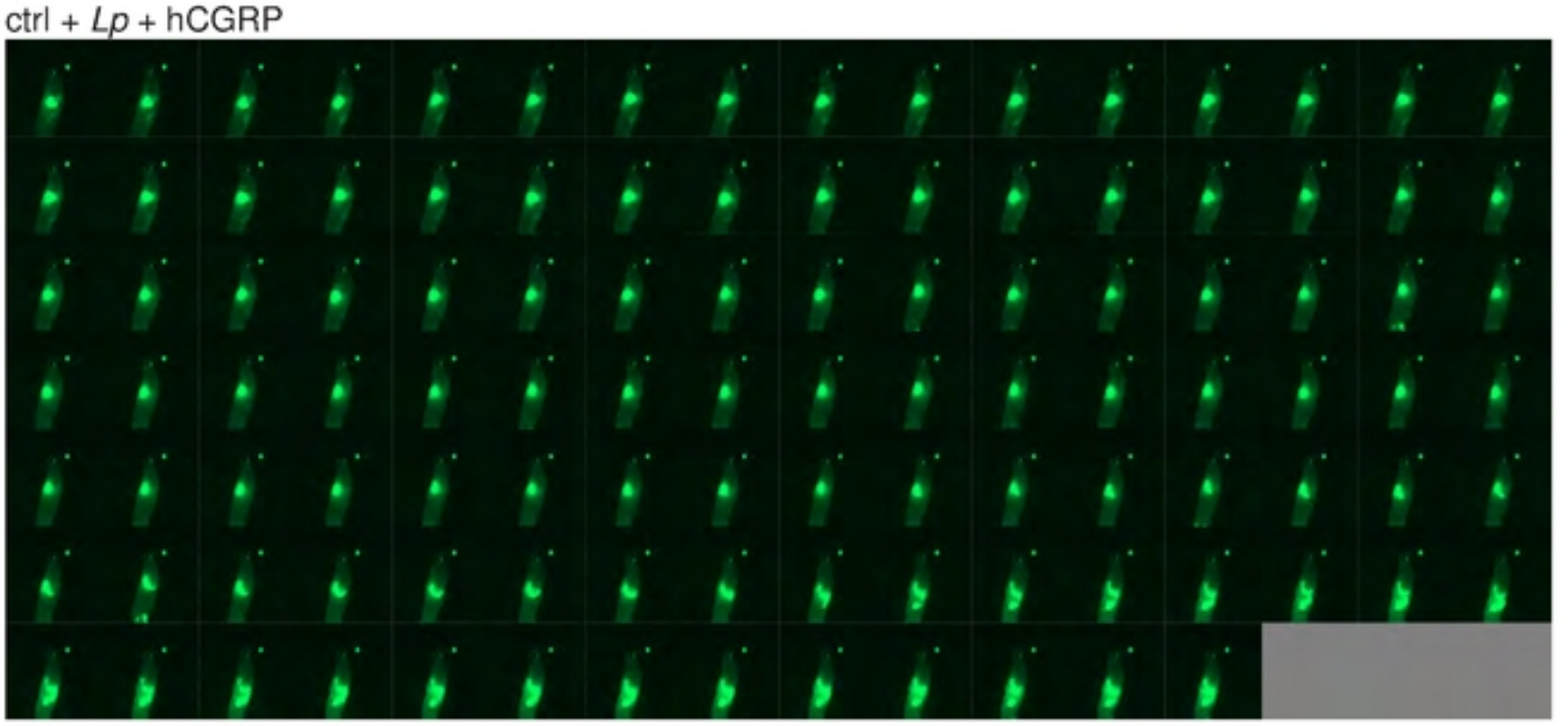

SUPP4

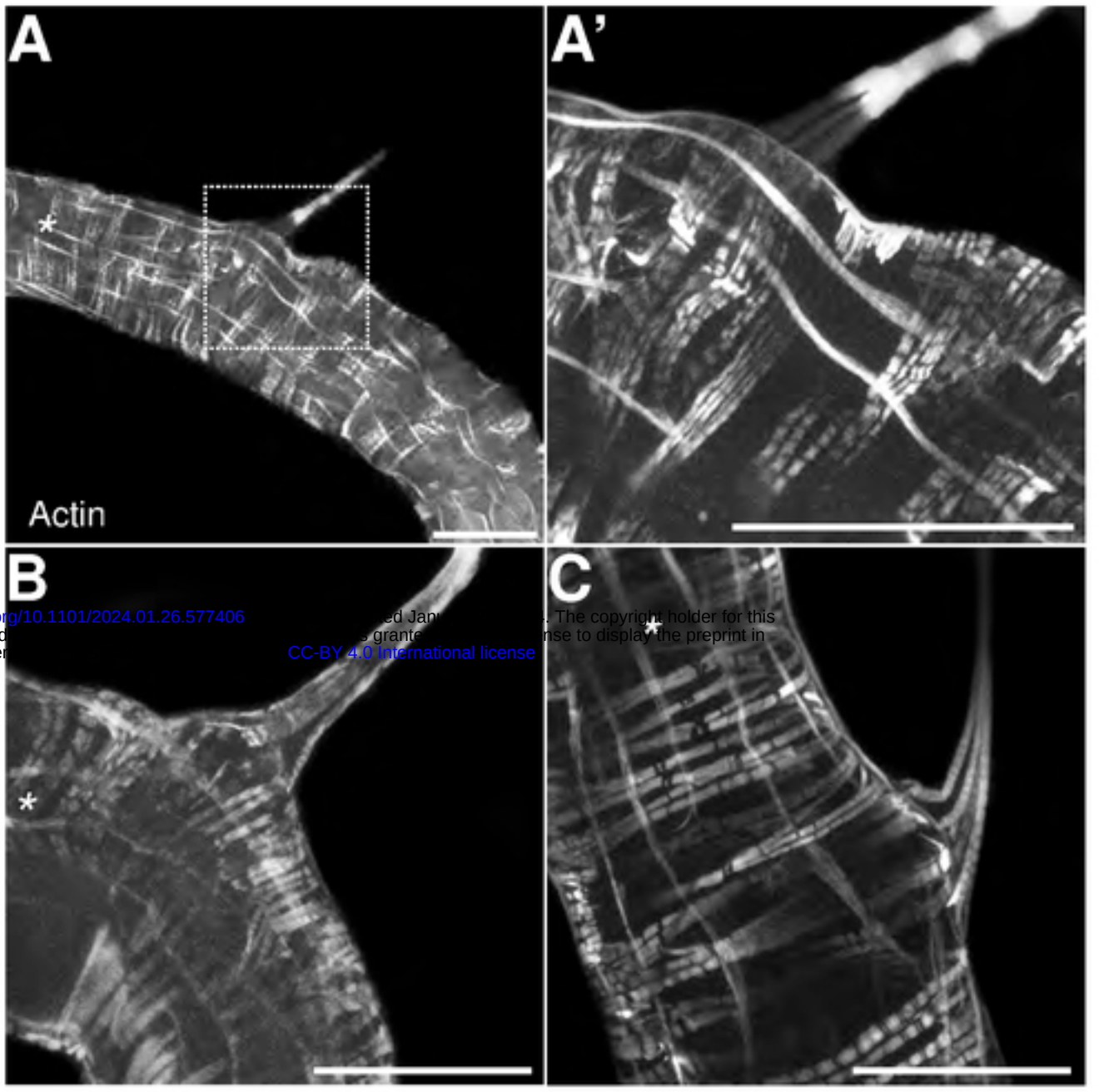

SUPP5

A *PGRP-LC$^{[\Delta E]}$ Bt*

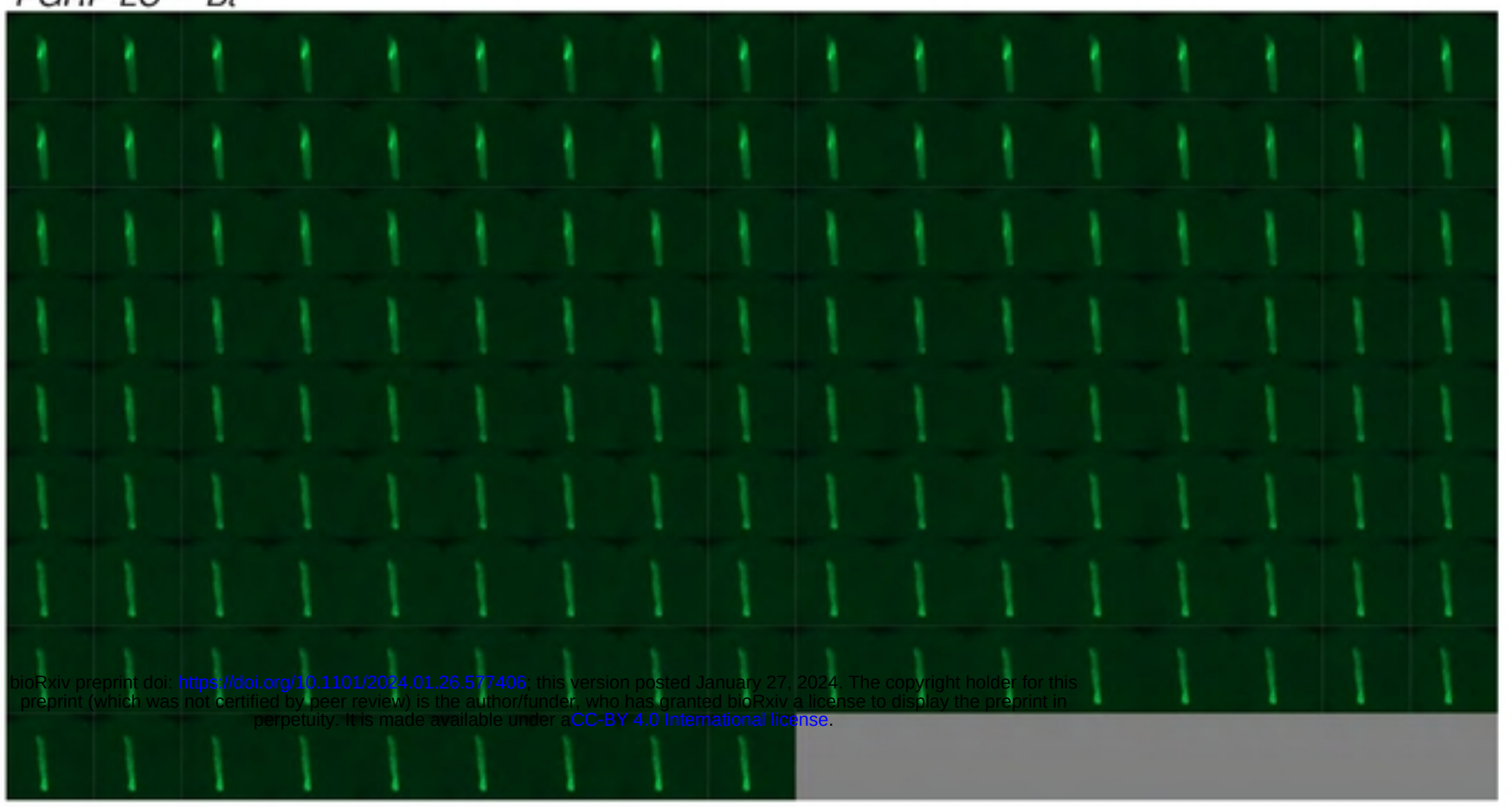

B *PGRP-LE$^{[112]}$ Ecc*

SUPP6

A *Dredd*[F64] *Ecc*

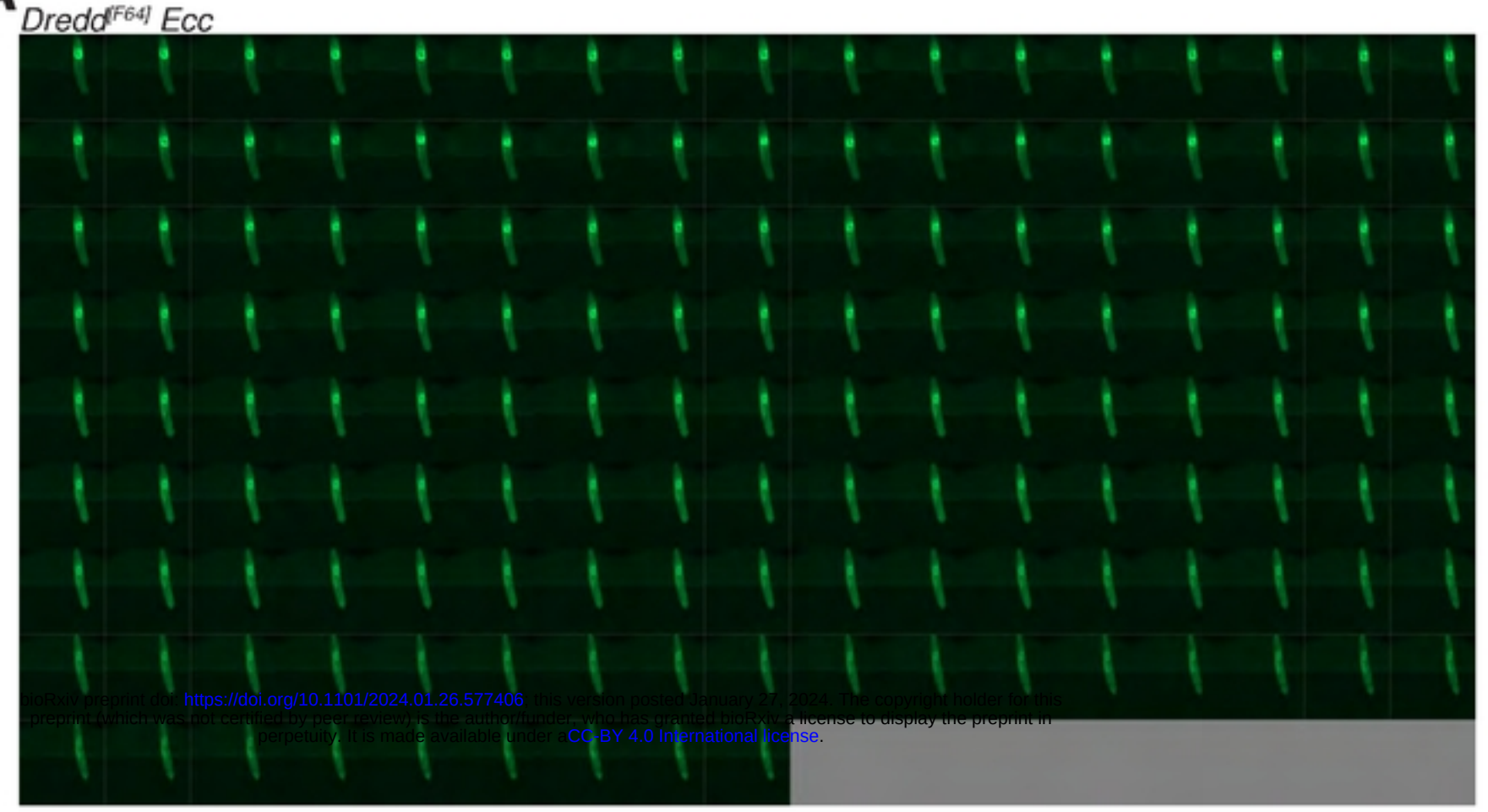

B *Rel*[E20] *Bt*

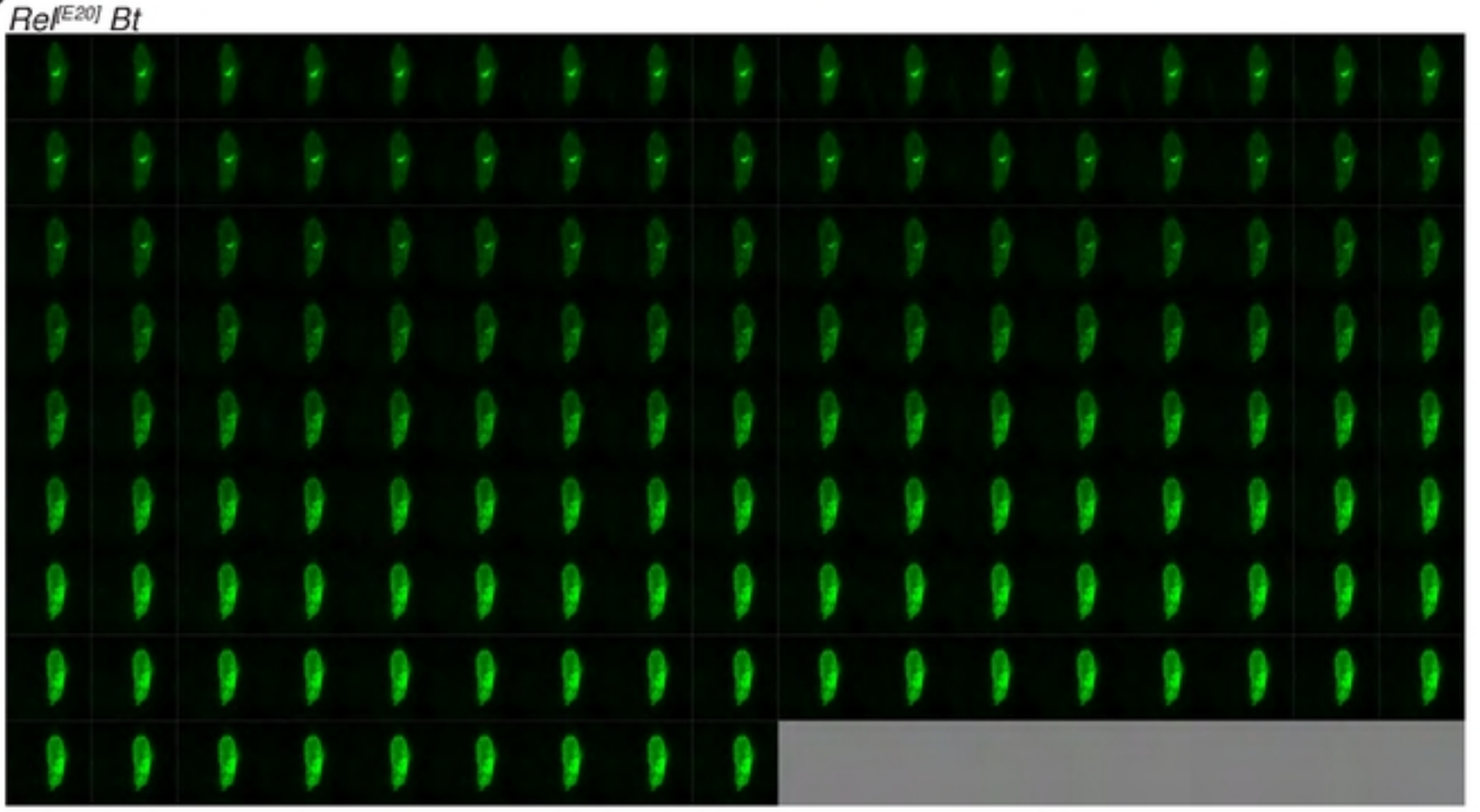

C *Rel*[E20] *Ecc*